ΠΟΛΥΤΕΧΝΕΙΟ ΚΡΗΤΗΣ

ΤΜΗΜΑ ΗΛΕΚΤΡΟΝΙΚΩΝ ΜΗΧΑΝΙΚΩΝ ΚΑΙ ΜΗΧΑΝΙΚΩΝ ΗΛΕΚΤΡΟΝΙΚΩΝ ΥΠΟΛΟΓΙΣΤΩΝ

Μελέτη της απόδοσης διαμορφώσεων υψηλής αποδοτικότητας σε περιβάλλον κινητής τηλεφωνίας

Όνομα Άρης Παπαδάκης

Ημερομηνία 04/08/2005

Table of Contents

Table of Figures

1 Introduction

As we continue to step forward into the new millennium with wireless technologies leading the way in which we communicate, it becomes increasingly clear that the dominant consideration in the design of systems employing such technologies will be their ability to perform with adequate margin over a channel perturbed by a host of impairments, not the least of which is multipath fading [1]. This is not to imply that multipath fading channels are something new to be reckoned with; indeed, they have plagued many a system designer for well over 40 years, but rather to serve as a motivation for their ever-increasing significance in the years to come.

Radio wave propagation through wireless channels is a complicated phenomenon characterized by various effects such as multipath and shadowing. A precise mathematical description of this phenomenon is either unknown or too complex for tractable communication systems analyses. However, considerable efforts have been devoted to the statistical modelling and characterization of these different effects. The result is a range of relatively simple and accurate statistical models for fading channels that depend on the particular propagation environment and the underlying communication scenario.

In this work Star QAM signal over fading channels will be discussed and their performance will be examined at slow and fast frequency flat fading channels. Initially Star QAM signals will be described and how they are derived from PSK and ASK modulations. Afterwards fading channels will be examined, and a statistical characterization will be given. Various forms of fading will be mentioned, such as slow and fast fading, flat and frequency selective fading, when they appear in mobile communications and what damage they do at the signal. The theoretical performance of Star MQAM frequency non-selective channels will be examined and closed form expressions for SER will be given. Simulations of 16 Star QAM signals over slow and fast fading channels will be carried out and graph results will be given. Finally an example of a frequency selective channel will be given by using a tapped delay line model to simulate it. A simple signal will be passed through the tapped delay line model and the consequences that frequency selective channels will be shown graphically.

2 QAM Modulation Scheme

The purpose of a communication system is to transmit information bearing signals (baseband signals) through a communication channel separating the transmitter from the receiver. The proper use of the communication channel requires a shift of the range of baseband frequencies into other frequency ranges suitable for transmission, and a corresponding shift back to the original frequency range after reception. A shift of the range of frequencies in a signal is accomplished by using modulation, which is defined as the process by which some characteristic of a carrier is varied in accordance with a modulating wave (signal). Modulation is performed at the transmitting end of the communication system. At the receiving end of the system, the original baseband signal is required to be restored. This is accomplished by using a process known as demodulation, which is the reverse of the modulation process.

In analogue modulation a sinusoidal carrier is used whose amplitude or angle is varied in accordance with a message signal and it is called continuous wave modulation.

In pulse modulation, some parameter of a pulse train is varied in accordance with the message signal [2]. There are two families of pulse modulation: analogue pulse modulation and digital pulse modulation. In analogue pulse modulation, a periodic pulse train is used as the carrier wave, and some characteristic feature of each pulse is varied in a continuous manner in accordance with the corresponding sample value of the message signal. In digital pulse modulation, the message signal is represented in a form that is discrete in both time and amplitude, thereby permitting its transmission in digital form as a sequence of coded pulses.

There is another way in which digital data may arise and this is as the output of a source of information that is inherently discrete in nature (e.g. a digital computer). Digital transmission may be done over a baseband channel or a pass band channel. Baseband transmission of digital data requires the use of a low-pass channel with a bandwidth large enough to accommodate the essential frequency content of the data stream.

In digital pass band transmission, the incoming data stream is modulated onto a carrier (usually sinusoidal) with fixed frequency limits imposed by a bandpass channel of interest. The communication channel used for passband data transmission may be a microwave radio link, a satellite channel etc. Yet other applications of

passband data transmission are in the design of passband line codes for use on digital subscriber loops and orthogonal frequency division multiplexing techniques for broadcasting. In any event, the modulation process making the transmission possible involves switching (keying) the amplitude, frequency, or phase of a sinusoidal carrier in some fashion in accordance with the incoming data. Thus there are three basic signaling schemes, and they are known as digital pulse amplitude modulation (PAM) or amplitude shift keying (ASK), frequency shift keying (FSK), and phase shift keying (PSK).

In the following paragraphs a detailed analysis of ASK and PSK will be carried out and a combination of these two methods will be done to produce a hybrid modulation called Quadrature amplitude modulation (QAM).

2.1 Pulse Amplitude Modulation (PAM)

In digital PAM, the signal waveforms may be represented as:

$$\begin{aligned} s_m(t) &= \mathrm{Re}[A_m g(t) e^{j2\pi f_c t}] \\ &= A_m g(t) \cos 2\pi f_c t \end{aligned} \quad m=1,2,\ldots,M,\ 0 \le t \le T \tag{2.1}$$

Where $\{A_m,\ 1 \le m \le M\}$ denote the set of M possible amplitudes corresponding to $M=2^k$ possible k-bit blocks or symbols. The signal amplitudes A_m take the discrete values (levels)

$$A_m = (2m-1-M)d\ ,\ m=1,2,\ldots,M \tag{2.2}$$

Where $2d$ is the distance between adjacent signal amplitudes [3]. The waveform $g(t)$ is a real-valued signal pulse whose shape influences the spectrum of the transmitted signal. The symbol rate for the PAM signal is R/k. This is the rate at which changes occur in the amplitude of the carrier to reflect the transmission of new information. The time interval $T_b=1/R$ is called bit interval and the time interval $T=k/R=kT_b$ is called the symbol interval.

The M-PAM signals have energies

$$\begin{aligned} E_m &= \int_0^T s_m^2(t)dt \\ &= \tfrac{1}{2} A_m^2 \int_0^T g^2(t)dt \\ &= \tfrac{1}{2} A_m^2 E_g \end{aligned} \tag{2.3}$$

Where E_g denotes the energy in the pulse *g(t)*. Clearly, these signals are one-dimensional, and are represented by the general form

$$s_m(t) = s_m f(t) \tag{2.4}$$

where *f(t)* is defined as the unit-energy signal waveform given as

$$f(t) = \sqrt{\frac{2}{E_g}} g(t) \cos 2\pi f_c t \tag{2.5}$$

and $$s_m = A_m \sqrt{\tfrac{1}{2} E_g}\ ,\ m=1,2,\ldots,M \tag{2.6}$$

The corresponding signal space diagrams for *M*=2, *M*=4, and *M*=8 are shown in Fig. 2.1.

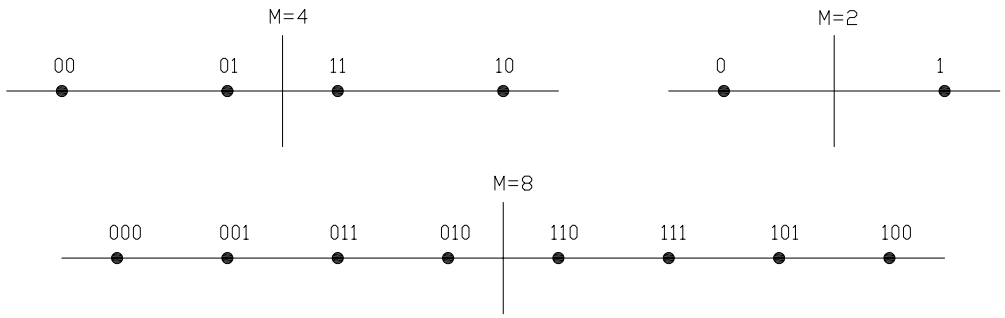

Fig. 2.1 Signal space diagram for digital PAM signals

The mapping of *k* information bits to the $M=2^k$ possible signal amplitudes is done by applying Gray encoding where the adjacent signals amplitudes differ by one binary digit as illustrated in Fig. 2.1.

The Euclidean distance between any pair of signal points is

$$\begin{aligned} d_{mn}^{(e)} &= \sqrt{(s_m - s_n)^2} \\ &= \sqrt{\tfrac{1}{2} E_g}\,|A_m - A_n| \\ &= d\sqrt{2E_g}\,|m-n| \end{aligned} \tag{2.7}$$

Hence the distance between a pair of adjacent signal points, i.e., the minimum Euclidean distance, is

$$d_{mn}^{(e)} = d\sqrt{2E_g} \tag{2.8}$$

2.2 Phase Shift Keying (PSK)

In digital phase modulation (PSK), the *M* signal waveforms are represented as

$$\begin{aligned} s_m(t) &= \mathrm{Re}[g(t)e^{j2\pi(m-1)/M}e^{j2\pi f_c t}] \\ &= g(t)\cos[2\pi f_c t + \theta_m] \qquad m=1,2,...,M,\ 0\le t \le T \\ &= g(t)\cos\theta_m \cos 2\pi f_c t - g(t)\sin\theta_m \sin 2\pi f_c t \end{aligned} \tag{2.9}$$

where $g(t)$ is the signal pulse shape and $\theta_m = 2\pi(m-1)/M,\ m=1,2,...,M,$ are the *M* possible phases of the carrier that convey the transmitted information

The energies of the signal waveforms are equal to:

$$\begin{aligned} E &= \int_0^T s_m^2(t)dt \\ &= \frac{1}{2}\int_0^T g^2(t)dt = \frac{1}{2}E_g \end{aligned} \tag{2.10}$$

The signal waveforms may be represented as a linear combination of two-orthogonal signal waveforms, $f_1(t)$ and $f_2(t)$, i.e.,

$$s_m(t) = s_{m1}f_1(t) + s_{m2}f_2(t) \tag{2.11}$$

where

$$\begin{aligned} f_1(t) &= \sqrt{\frac{2}{E_g}}g(t)\cos 2\pi f_c t \\ f_2(t) &= -\sqrt{\frac{2}{E_g}}g(t)\sin 2\pi f_c t \end{aligned} \tag{2.12}$$

And the two dimensional vectors $\mathbf{s}_m = [s_{m1}\ s_{m2}]$ are given by

$$\mathbf{s}_m = \left[\sqrt{\frac{E_g}{2}}\cos\frac{2\pi}{M}(m-1) \qquad \sqrt{\frac{E_g}{2}}\sin\frac{2\pi}{M}(m-1)\right], \qquad m = 1,2,...,M \tag{2.13}$$

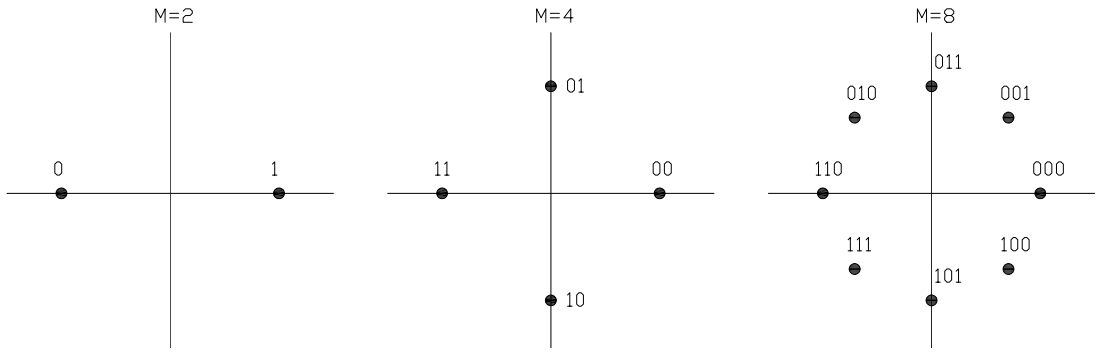

Fig. 2.2 Signal space diagrams for PSK signals

In Fig. 2.2 the signal space diagrams for M=2, 4, and 8 are shown where it can be seen that for M=2 the PSK signal is identical to the Binary PAM signal [3]. The mapping of k information bits are Gray encoded as in the case of PAM.

The Euclidean distance between signal points is:

$$\begin{aligned} d_{mn}^{(e)} &= \left|\mathbf{s}_m - \mathbf{s}_n\right| \\ &= \left\{ E_g \left[1 - \cos\frac{2\pi}{M}(m-n) \right] \right\}^{1/2} \end{aligned} \tag{2.14}$$

The minimum Euclidean distance corresponds to the case in which $|m\text{-}n|$=1, i.e. adjacent signal phases. In this case,

$$d_{mn}^{(e)} = \sqrt{E_g \left(1 - \cos\frac{2\pi}{M} \right)} \tag{2.15}$$

2.3 Quadrature Amplitude Modulation (QAM)

In an M-ary PSK system, the in-phase and quadrature components of the modulated signal are interrelated in such a way that the envelope is constrained to remain constant. The constraint manifests it self in a circular constellation for the message points. However, if this constraint is removed, and the in-phase and quadrature components are thereby permitted to be independent, we get a new modulation scheme called M-ary quadrature amplitude modulation (QAM). This latter modulation scheme is hybrid in nature in that the carrier experiences amplitude as well as phase modulation.

QAM is used in NTSC and PAL television systems, where the in-phase and 90° components carry the components of color information. It is also used extensively in modems, and other forms of digital communication over analogue channels. 64-QAM and 256-QAM are often used in digital cable television and cable modem applications. In the US, 64-QAM and 256-QAM are the mandated modulation schemes for digital cable, as standardized by the SCTE in the standard ANSI/SCTE 07 2000.

The bandwidth efficiency of PAM/SSB can also be obtained by simultaneously impressing two separate k-bit symbols from the information sequence $\{a_n\}$ on two quadrature carriers $\cos 2\pi f_c t$ and $\sin 2\pi f_c t$. The resulting modulation technique is called quadrature PAM or QAM, and the corresponding signal waveforms may be expressed as:

$$\begin{aligned} s_m(t) &= \mathrm{Re}[(A_{mc} + jA_{ms})g(t)e^{j2\pi f_c t}], \qquad m = 1,2,...,M \\ &= A_{mc}g(t)\cos 2\pi f_c t - A_{ms}g(t)\sin 2\pi f_c t, \quad 0 \le t \le T \end{aligned} \tag{2.16}$$

Where A_{mc} and A_{mc} are the information bearing signal amplitudes of the quadrature carriers and *g(t)* is the signal pulse.

Alternatively, the QAM signal waveforms may be expressed as:

$$\begin{aligned} s_m(t) &= \mathrm{Re}[V_m e^{j\theta_m} g(t)e^{j2\pi f_c t}] \\ &= V_m g(t)\cos(2\pi f_c t + \theta_m) \end{aligned} \tag{2.17}$$

Where $V_m = \sqrt{A_{mc}^2 + A_{ms}^2}$ and $\theta_m = \tan^{-1}(A_{ms}/A_{mc})$. From this expression, it is apparent that the QAM signal waveforms may be viewed as combined amplitude and phase modulation.

Any combination of M_1-level PAM and M_2-phase PSK may be selected to construct a $M=M_1M_2$ combined PAM-PSK signal constellation [3]. If $M_1=2^n$ and $M_2=2^m$, the combined PAM-PSK signal constellation results in the simultaneous transmission of $m+n=\log M_1M_2$ binary digits occurring at a symbol rate $R/(m+n)$. In Fig. 2.3 signal space diagrams for combined PAM-PSK are shown.

As in the case of PSK signals, the QAM signal waveforms may be represented as a linear combination of two orthonormal signal waveforms, $f_1(t)$ and $f_2(t)$:

$$s_m(t) = s_{m1}f_1(t) + s_{m2}f_2(t) \tag{2.18}$$

where

$$\begin{aligned} f_1(t) &= \sqrt{\frac{2}{E_g}}g(t)\cos 2\pi f_c t \\ f_2(t) &= -\sqrt{\frac{2}{E_g}}g(t)\sin 2\pi f_c t \end{aligned} \tag{2.19}$$

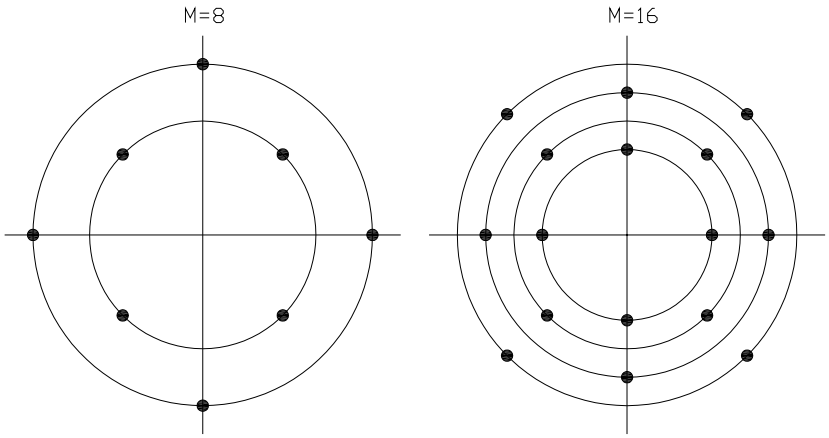

Fig. 2.3 Examples of combined PAM-PSK signal space diagrams

and

$$\begin{aligned}\mathbf{s}_m &= [s_{m1} \quad s_{m2}] \\ &= \left[A_{mc}\sqrt{\tfrac{1}{2}E_g} \quad A_{ms}\sqrt{\tfrac{1}{2}E_g}\right]\end{aligned} \tag{2.20}$$

E_g is the energy of the signal pulse *g(t)*.

The Euclidean distance between any pair of signal vectors is

(2.21)

$$\begin{aligned}d_{mn}^{(e)} &= \left|\mathbf{s}_m - \mathbf{s}_n\right| \\ &= \sqrt{\tfrac{1}{2}E_g[(A_{mc}-A_{nc})^2 + (A_{ms}-A_{ns})^2]}\end{aligned} \tag{2.22}$$

In the special case where the signal amplitudes takes the set of discrete values {(*2m-1-M)d, m=1,2,...,M*} the signal space diagram is rectangular. In this case the modulation is called Square QAM and the Euclidean distance between adjacent points is:

$$d_{mn}^{(e)} = d\sqrt{2E_g} \tag{2.23}$$

which is the same result as for PAM

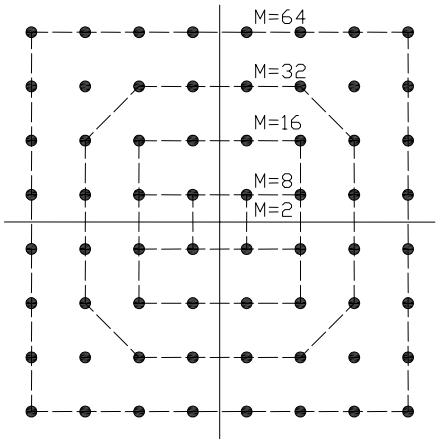

Fig. 2.4 Several signal space diagrams for square QAM

From Fig. 2.4 it can be seen that in 16-state Quadrature Amplitude Modulation (16QAM), there are four in phase *I* values and four quadrature *Q* values. This results in a total of 16 possible states for the signal. It can transition from any state to any other state at every symbol time. Since $16 = 2^4$, four bits per symbol can be sent. This consists of two bits for *I* and two bits for *Q*. The symbol rate is one fourth of the bit rate. So this modulation format produces a more spectrally efficient transmission. It is more efficient than BPSK, QPSK, or 8PSK. Note that QPSK is the same as 4QAM. Another variation is 32QAM. In this case there are six *I* values and six *Q* values resulting in a total of 36 possible states (6x6=36). This is too many states for a power of two (the closest power of two is 32). So the four corner symbol states, which take the most power to transmit, are omitted. This reduces the amount of peak power the transmitter has to generate. Since $2^5 = 32$, there are five bits per symbol and the symbol rate is one fifth of the bit rate. The current practical limits are approximately 256QAM, though work is underway to extend the limits to 512 or 1024 QAM. A 256QAM system uses 16 *I*-values and 16 *Q*-values, giving 256 possible states. Since $2^8 = 256$, each symbol can represent eight bits. A 256QAM signal that can send eight bits per symbol is very spectrally efficient. However, the symbols are very close together and are thus more subject to errors due to noise and distortion. Such a signal may have to be transmitted with extra power (to effectively spread the symbols out more) and this reduces power efficiency as compared to simpler schemes.

2.3.1 Star QAM Constellation

Digital communications using 16-level QAM signals and conventional receiver techniques have unacceptably high BER in a Rayleigh fading environment [4]. The problem is the inability to track absolute phase during fades with the result that on emergence from a fade the phase locked loop (PLL) in the receiver locks onto a different quadrant than that required [5]. Differential encoding can reduce this false phase locking problem, but the standard square QAM constellation suffers from possible false lock positions at 26^o and 53^o. At these angles, given appropriate amplitude scaling, more than half the original constellation points can be successfully mapped onto the rotated constellation points. The points that cannot be successfully mapped cause random fluctuations in the error signal in the clock recovery loop but do not actually drive the system off lock. Data mapped onto these points will nearly always be in error and thus this problem cannot be overcome with differential coding. Unfortunately, false locking occurs fairly frequently as the PLL and automatic gain control (AGC) tend to drive the system towards these lock points. The AGC can pose a problem for the square constellation as it has to act very fast to follow the fades, yet at the same time it must maintain a high degree of accuracy to allow amplitude information to be correctly decoded.

A constellation having no false lock positions is introduced in [6] to overcome these deficiencies. This constellation is called 'Star QAM' and is shown in Fig. 2.5, it does not have a minimum least free distance between points in the strict sense, but does allow efficient differential encoding and decoding methods to be used which go some way toward mitigating the effects of Rayleigh fading.

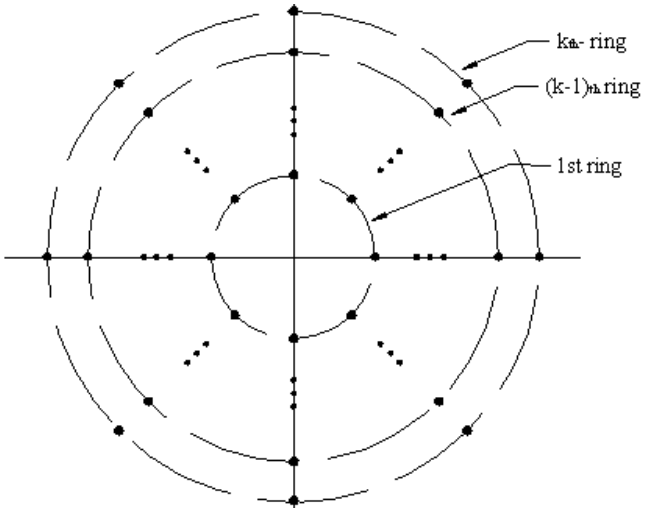

Fig. 2.5 Constellation of M-ary Star QAM

Some form of differential encoding is essential with PLLs as the Rayleigh fading channel can introduce phase shifts in excess of 50^{o} between consecutive symbols, making it extremely difficult to establish an absolute phase reference. The differential encoding system considerably improves the BERs compared with those for the square constellation because it eliminates long error bursts that occur when a false lock has been made. Of considerable importance is that with differential amplitude encoding there is no longer any need for AGC. This not only simplifies the circuit but also removes errors caused by an inability of the AGC to follow the fading envelope. Since Star QAM was first introduced a lot of research has been carried out [7, 8, 9, 10, 11, 12]. Its applications may include light weight hand held portable telephones, where power consumption, weight and low cost construction are crucial issues, and hence lower complexity modem schemes are desirable. In this case it may be preferable to reduce the system performance slightly in order to be able to employ a low- complexity non- coherent differentially encoded QAM constellation, such as the circular or star QAM scheme [13].

In the following chapters fading channels will be examined in detail and symbol error rate expressions will be derived for Star QAM in fading channels.

3 Characterization of fading channels

3.1 The additive white Gaussian noise channel

In the design of communication systems for transmitting information through physical channels, it is convenient to construct mathematical models that reflect the most important characteristics of the transmission medium. Then the mathematical model for the channel is used in the design of the channel encoder and the modulator at the transmitter and the demodulator and channel decoder at the receiver. A simple mathematical model is the additive noise channel where the transmitted signal is corrupted by an additive random noise process. Physically the additive noise process may arise from electronic components and amplifiers at the receiver of the communication system or from interference encountered in transmission. This type of noise is characterized statistically as a Gaussian noise process and the resulting mathematical model is called the additive Gaussian noise channel.

An idealized form of noise is white noise where its power spectral density is independent of the operating frequency. The adjective white is used in the sense that white light contains equal amounts of all frequencies within the visible band of electromagnetic radiation. Two different samples of white noise, no matter how closely together in time are taken, are uncorrelated. If the white noise is also Gaussian, then the two samples are statistically independent. The combination of white and Gaussian noise gives the classical additive white Gaussian noise channel (AWGN) which represents the ultimate in “randomness”.

3.2 Examples of time variant multipath communication channels

The Gaussian noise channel is inadequate in characterizing signal transmission over radio channels whose transmission characteristics change with time. In such cases, a more general mathematic model must be developed, that characterize the time varying behavior of the channel [14]. Some examples of communication channels that require a different kind of channel model are given below.

3.2.1 Signal transmission via ionospheric propagation in the HF band.

Because of the ionospheric layers, the signal arrives at the receiver via different propagation paths at different delays these signal components are called multipath components. The signal multipath components generally have different carrier-phase

offsets and, hence, they may add destructively at times, resulting in a phenomenon called signal fading.

3.2.2 Mobile cellular transmission

In mobile cellular transmission between a base station and a mobile phone or a telephone equipped automobile, the signal transmitted from the base station arrives at the mobile through several reflections from the surrounding buildings, hills and other obstructions with consequences which affect the signal power, since the signal arrives from many propagation paths at different delays which adds constructively or destructively. The same is true of transmission from the automobile to the base station. Moreover, the speed that the automobile is traveling results in frequency offsets, called Doppler shifts, of the various frequency components of the signal.

3.2.3 Line of sight microwave radio transmission

In line-of-sight (LOS) radio transmission of signals, the transmitting and receiving antennas general1y are mounted on high towers, to avoid obstructions such as buildings and hills in the path of signa1 propagation. However, when there are tall obstructions or hilly terrain in the path of propagation, it is likely that signals will be reflected from the ground to the receiving antenna. This is especially a problem under severe weather conditions. In this case there is a received signal component that arrives via the direct path and an ensemble of secondary paths that are reflected from the ground terrain. The latter arrive at the receiver with various delays and constitute multipath propagation. Relatively narrow-beamwidth antennas are employed in microwave LOS transmission to reduce the occurrence of secondary reflections. Nevertheless, some secondary signal reflections are frequently observed in practice.

3.2.4 Airplane to airplane radio communications

in radio communications between two aircrafts, it is possible for secondary signal components to be received from ground reflections. This is especially the case when omni-directional antennas are employed in the communication system. The ensemble of ground-reflected signal components generally arrive at the receiver with different delays and different attenuations. In addition, the motions of the aircraft result in Doppler frequency offsets in the various signal components. In many respects, this situation is similar to that in mobile cellular communications.

3.3 Physical Basis of Fading

In a multipath environment as it is shown in Fig. 3.1, the composite received signal is the sum of the signals arriving along different paths. Except for the LOS path, all paths are going through at least one order of reflection, transmission, or diffraction before arriving at the receiver.

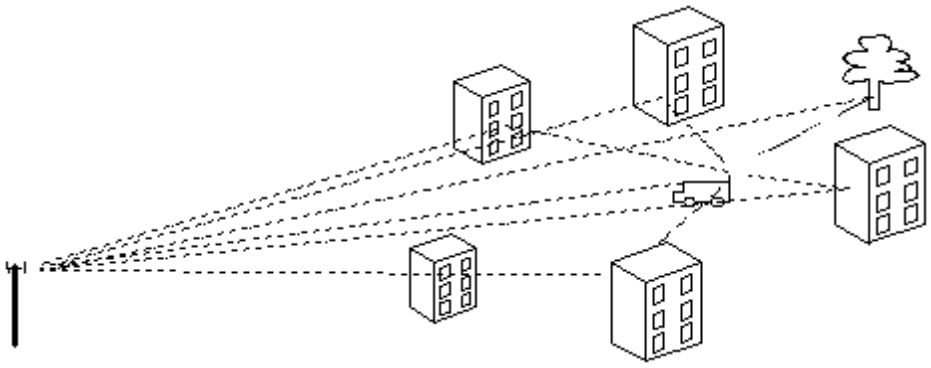

Fig. 3.1 Typical link between mobile and base station antennas

The LOS path is the first to arrive and it is usually the strongest of the individual paths but it is not necessarily stronger than the aggregate of the scattered paths. Since the individual paths are linear (i.e, they satisfy the superposition requirements), the overall multipath channel is linear. Each path has its own delay and gain/ phase shift, so the aggregate of paths can be described by its impulse response or frequency response. Therefore different carrier frequencies will experience different gains and phase shifts [15]. The modulation of the carrier depends on the time scale of the modulation (roughly, the reciprocal of its bandwidth), and is significantly effected by the range of delays (the "delay spread"). This implies that the dimensionless product of channel delay spread and signal bandwidth is an important measure. If the mobile changes position, the paths all change length in varying amounts. Since a change in path length of just one wavelength produces 2π radians of phase shift, a displacement of a fraction of a wavelength in any direction causes a large change in the aggregate gain and phase shift, as the sum of the paths shifts between reinforcement and cancellation.

When the mobile moves through this two dimensional standing wave pattern, the impulse response and frequency response change with time, so the channel is a time-varying linear filter. The time variant nature of the net gain is termed "fading" and the fastest rate of change is the "Doppler frequency". The modulation of the carrier depends on the time span of the required receiver processing (eg, differential

detection over two symbols, equalization over many symbols), and is significantly effected by the time-varying nature of fading. The dimensionless product of this time span and the Doppler frequency is another important parameter.

Either or both fading and delay spread can be significant or not in a given terrain with a given modulation rate. Fading is expected to be rapid with vehicular use, but modest with pedestrian use. Similarly, delay spread can be large in hilly or mountainous terrain, but smaller in an urban core, where multiple reflections quickly attenuate the signals with longer path lengths.

3.4 Mathematical Model of Fading

Radio signals are always bandpass, and are almost always narrowband. The transmitted bandpass signal at carrier frequency f_c with complex envelope $s(t)$ is denoted by

$$s'(t) = \mathrm{Re}\left(s(t) \cdot e^{2 \cdot \pi \cdot j \cdot f_c \cdot t} \right) \tag{3.1}$$

In a multipath environment there will be many signals arriving at the receiver each with its own reflection coefficient, $\alpha_i(t)$, and propagation delay $\tau_i(t)$.

If there are i signals arriving from the scatterers the received bandpass signal will be described from the equation:

$$y'(t) = \sum_i a_i(t) \cdot s'(t - \tau_i(t)) \tag{3.2}$$

By substituting equation (3.1) in (3.2) yields the result

$$y'(t) = \mathrm{Re}\left\{ \left[\sum_i a_i(t) \cdot e^{-j 2\pi f_c \tau_i(t)} s(t - \tau_i(t)) \right] \cdot e^{j 2\pi f_c t} \right\} \tag{3.3}$$

The equivalent low pass signal of (3.3) is

$$y(t) = \sum_i a_i(t) \cdot e^{-j 2\pi f_c \tau_i(t)} s(t - \tau_i(t)) \tag{3.4}$$

And (3.3) can be simplified to

$$y'(t) = \mathrm{Re}\left(y(t) \cdot e^{2 \cdot \pi \cdot j \cdot f_c \cdot t} \right) \tag{3.5}$$

When the mobile moves through this welter of arriving reflections, the path lengths change. If the angle of arrival of path i with respect to the direction of motion is θ_i, then the path length change, as a function of speed v and time t is

$$\Delta x_i = -v \cos(\theta_i) \cdot t \tag{3.6}$$

This shifts the frequency of each component by an amount dependent on its arrival angle θ_i as it is shown below. By taking $\tau_i=(x_i+\Delta x_i)/c$, and $f_c=c/\lambda$, (3.6) and substituting them in (3.4) we have

$$\begin{aligned} y(t) &= \sum_i a_i(t)\cdot e^{-j2\pi\cdot\frac{(x_i+\Delta x_i)}{\lambda}} s\left[t-\frac{(x_i+\Delta x_i)}{c}\right] \\ &= \sum_i a_i(t)\cdot e^{-j2\pi\cdot\frac{x_i}{\lambda}}\cdot e^{j2\pi\cdot\frac{v\cos(\theta_i)t}{\lambda}} s\left[t-\frac{x_i}{c}+\frac{v\cos(\theta_i)t}{c}\right] \end{aligned} \tag{3.7}$$

Where c is the speed of light, and λ is the wavelength.

The above equation may be simplified if the phases $2\pi x_i/\lambda$ is included in the phase of a_i because it is constant, and the term $v\cos(\theta_i)t/c$ is neglected since this delay is very small compared with the time scale of the modulation $s(t)$.

$$\begin{aligned} y(t) &= \sum_i a_i(t)\cdot e^{j2\pi\cdot\frac{v\cos(\theta_i)t}{\lambda}} s\left(t-\frac{x_i}{c}\right) \\ &= \sum_i a_i(t)\cdot e^{j2\pi\cdot f_d\cos(\theta_i)t} s\left(t-\tau_i\right) \end{aligned} \tag{3.8}$$

In the above equation it is shown that the i^{th} scatterer shifts the input signal in time by τ_i, and in frequency by $f_d\cos(\theta_i)$. the maximum Doppler shift is $f_d=v/\lambda$.

In flat fading the signal bandwidth is so small that the delays τ_i do not affect the signal, and $s(t-\tau_i) \approx s(t)$. In frequency selective fading the signal bandwidth is bigger and the delays affect the signal.

3.5 Consequences of a multipath channel

In the previous section a multipath channel model was described mathematically by (3.8). The consequences of that equation are Doppler spread f_d which is produced by vehicle motion and delay spread τ_i which is produced by the delays of the reflections of the signal. They are produced by two separate mechanisms, and either of them can be present or absent in common mobile situations.

3.5.1 Doppler Spread

Whenever a transmitter and a receiver are in relative motion, the received carrier frequency is shifted relative to the transmitted carrier frequency. This shifting of frequency is the **Doppler effect** of wave propagation between nonstationary points.

If we consider that the portable terminal is moving with speed v, then the path lengths of the arriving reflections change. **Doppler frequency spread** is a measure of how rapidly the signal is changing with time. If the signal changes slowly the Doppler

frequency spread is relatively small, while if the signal changes rapidly the Doppler frequency spread is large.

If we assume flat fading, in which the signal bandwidth is so small that the delays τ_i do not affect the signal as it will be explained below, equation (3.8) will become

$$y(t) = s(t) \cdot \sum_i a_i(t) \cdot e^{j2\pi \cdot f_d \cos(\theta_i)t} = g(t) \cdot s(t) \tag{3.9}$$

Where the channel complex gain *g(t)* is time varying because the phase angles $2\pi f_d cos(\theta_i)t$ change with time. This means that the Doppler effect and the variation of gain with time are relative to the motion of the mobile. The complex gain *g(t)* may become zero or close to zero while time varies and that has as a result the fade of the received signal *y(t)*.

In a realistic indoor environment the received signal arrives from several reflected paths with different path distances, and the velocity of movement in the direction of each arriving path is generally different from that of another path. Thus a transmitted signal instead of being subjected to a simple Doppler shift is received as a spectrum which is referred as the Doppler spectrum of Doppler spread.

The received signal is affected by the complex gain and this depends on the fade rate and the time span of the required receiver processing. If the complex gain does not change significantly over this time span, then the primary effect is just a slowly varying SNR. This condition is termed **slow fading** and the criterion is that the product of fade rate and processing window is very small, that is $Nf_dT<<1$, where *N* is the receiver processing window measured in symbols and *T* is the symbol duration.

If this product is significant, so that the signal in the window, or even individual data pulses, are distorted then this phenomenon is termed **fast fading.** In that case errors are produced even if there is no noise and no increase in power will eliminate it.

3.5.2 Delay Spread

If the transmitted signal is an impulse in time, the reflections spread it out upon reception. This range of delays, which is called **delay spread**, causes variation of the frequency response of the signal. Significant variation of the frequency response across the band produces signal distortion which will show up as intersymbol interference (ISI). At certain frequencies it is possible to have deep nulls, so part of the signal can be notched out. This is called **frequency selective transmission** and if the range of delays is not significant, the channel is considered flat. The criterion to

distinguish flat from frequency selective transmission is the comparison between delay spread and the fine structure in time of the signal (the reciprocal bandwidth of the signal). If the delay spread is very small compared to the reciprocal bandwidth we have frequency flat transmission, that is $\tau_d W << 1$.
Mathematically delay spread may be expressed as

$$y(t) = \sum g_i(t) \cdot s(t - \tau_i) \text{ where } g_i(t) = a_i \cdot e^{j\phi_i}$$

where very small Doppler or a stationary mobile is assumed and the phases of the reflections can be considered constant. In Fig. 3.2 the impulse response of a signal is shown where the signal is an impulse in time and its response spreads out in time because of the reflections.

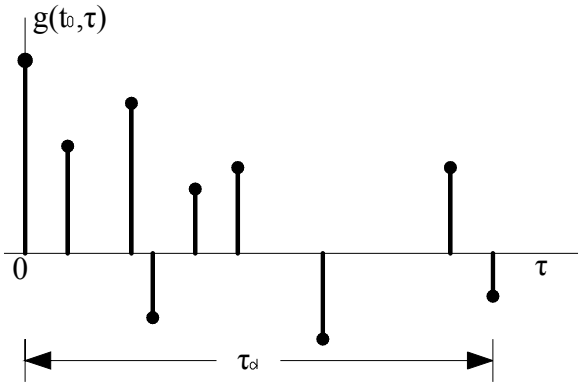

Fig. 3.2 Impulse response of a signal

If both of the above phenomena are present, Doppler and delay spread, then we have frequency selective fading and it is described by the following formula

$$y(t) = \sum g_i(t) \cdot s(t - \tau_i) \text{ where } g_i(t) = a_i \cdot e^{j \cdot 2 \cdot \pi \cdot f_d \cdot \cos(\theta_i) \cdot t}$$

This is a difficult situation for modulation and detection, especially if the fading is fast. This channel is a time variant linear filter. This means that the channel has an impulse response that depends on observation time *t*, as well as the delay *τ*.

3.6 Fading Statistics

In fading the received signal consists of a large number of copies of the transmitted signal, each with its own amplitude, phase and path delay, so all we have to do to know the relationship between the transmitted and the received signals is to measure the reflection coefficients and path lengths. But in practice, there are so many paths

that this is impractical. In addition there will be some inevitable errors in path length measurements, which even if they are really small (fraction of a wavelength), they introduce phase shifts that make the resultant quite different from the prediction. In such cases a statistical description is used, so that even if the actual channel filtering is not known some of its average properties can be characterized.

3.6.1 Rayleigh Fading

There are several probability distributions that can be considered in attempting to model the statistical characteristics of the fading channel. When there are a large number of scatterers in the channel that contribute to the signal at the receiver, as is the case in ionospheric or tropospheric signal propagation, application of the central limit theorem leads to a Gaussian process model for the channel impulse response. If the process is zero-mean, then the envelope of the channel response at any time instant has a Rayleigh probability distribution and the phase is uniformly distributed in the interval (0,2π). That is:

$$p_r(r) = \frac{r}{\sigma_g^2} e^{\left(-\frac{r^2}{2\sigma_g^2}\right)} \tag{3.10}$$

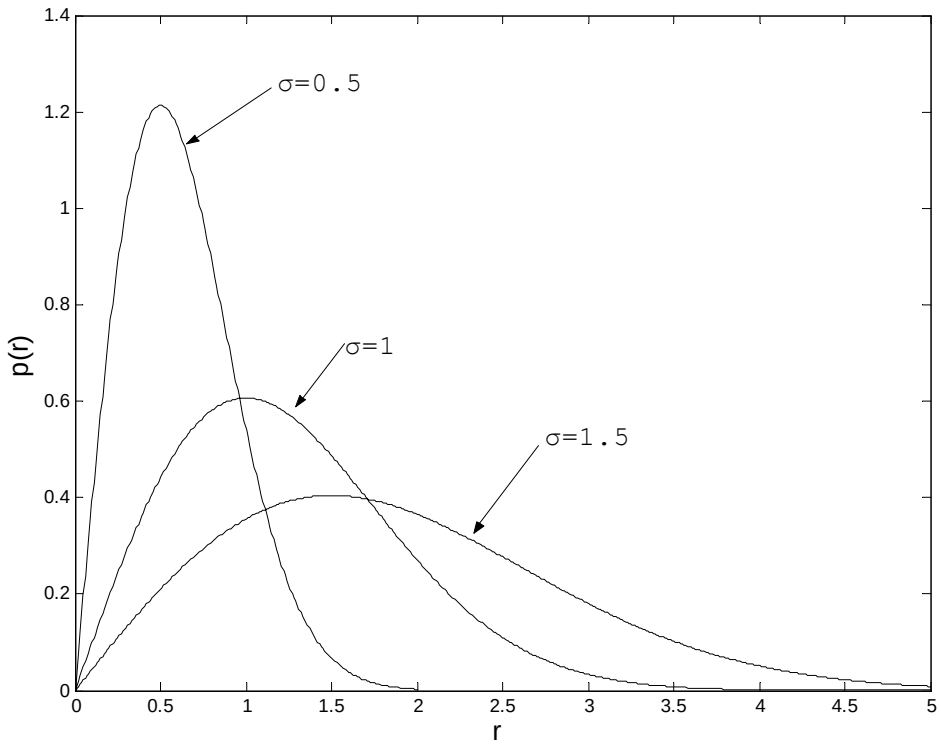

Fig. 3.3 Distribution of Rayleigh fading for various values of σ_g

3.6.2 Rice Fading

There are many radio channels in which fading is encountered that are basically line-of-sight (LOS) communication links with multipath components arising from secondary reflections, or signal paths, from surrounding terrain. In such channels, the number of multipath components is small, and hence the channel may be modeled in a somewhat simpler form. These channels may be described by the Rice distribution where the total gain is the sum of a constant specular (or LOS or discrete) component g_s and a zero mean Gaussian diffuse (or scattered) component g_d, so that g is a nonzero mean Gaussian variate.

$g=g_s+g_d$

The specular component has K times the power of the diffuse component (the Rice K-factor), so that K=0 gives Rayleigh fading and K==>∞ gives a constant channel.

The pdf of the Rician distribution is given by:

$$p_r(r,K) = \frac{r}{\sigma^2} e^{\left(-\frac{r^2}{2\sigma^2}-K\right)} \cdot I_o\left(\frac{r\sqrt{2\cdot K}}{\sigma}\right) \tag{3.11}$$

Where I_0 is the modified Bessel function of the first kind.

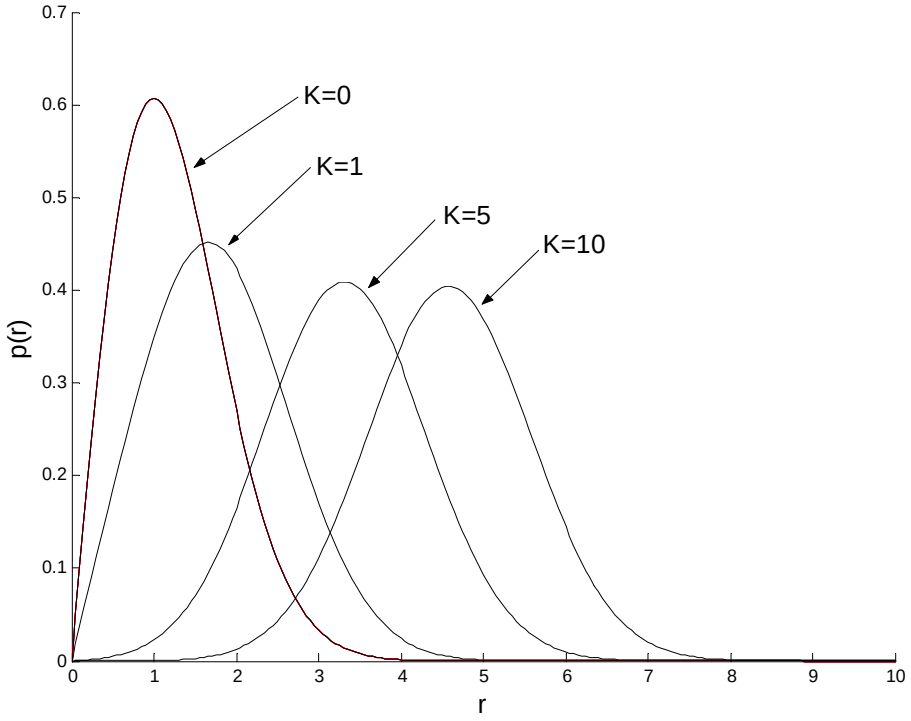

Fig. 3.4 Distribution of Rice fading for various values of K

From the graph we can see that for large K the graph can be approximated by the Gaussian pdf.

3.6.3 Nakagami-m Fading

An alternative statistical model for the envelope of the channel response is the Nakagami-m distribution given by the pdf:

$$p_r(r,m) = \frac{2}{\Gamma(m)} \cdot \left(\frac{m}{2 \cdot \sigma^2} \right)^m \cdot r^{2 \cdot m - 1} \cdot e^{\frac{-m \cdot r^2}{2 \cdot \sigma^2}} \tag{3.12}$$

Where m is the order of the pdf, $2\sigma^2$ is the mean square value and $\Gamma(m)$ is the gamma function (equal to (m-1)! for integers).

In contrast to the Rayleigh distribution, which has a single parameter that can be used to match the fading channel statistics, the Nakagami-m is a two parameter distribution involving the parameter m and the mean square value $2\sigma^2$. As a consequence, this distribution provides more flexibility and accuracy in matching the observed signal statistics. The Nakagami-m distribution can be used to model fading channel conditions that are either more or less severe than the Rayleigh distribution, and it includes the Rayleigh distribution as a special case (m=1).

By increasing the order m of the Nakagami distribution changes its character from that of a purely scattered fading to fading with a LOS component. For modeling these channels, it is therefore a reasonable alternative to the Rice pdf which it resembles. For larger values of m, just as for larger values of K in the Rice pdf, it can be approximated by a Gaussian pdf

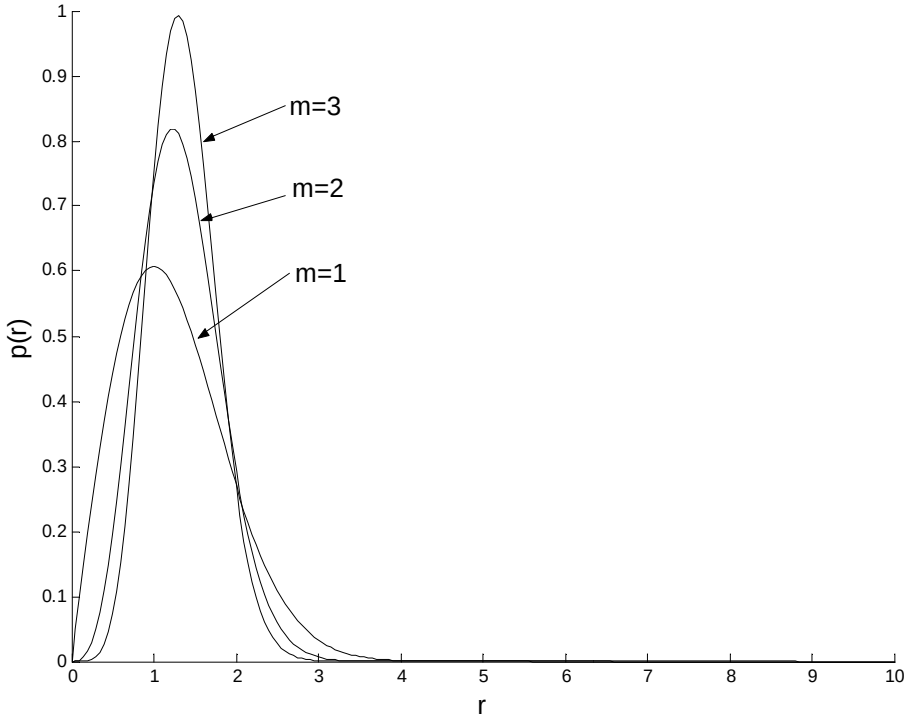

Fig. 3.5 Nakagami-m fading for various values of m

3.7 Second order statistics of time selective, flat fading channels

In flat fading channels, as it was discussed before, the power spectrum of the output signal is broadened by the Doppler shifts because of the complex gain process *g(t)*. This Doppler spectrum represents the distribution of scatterers (density of power) in the Doppler domain λ. The process *g(t)* is assumed to be wide sense stationary (WSS) that is that scatterers at different Dopplers are uncorrelated. The Doppler spectrum and the autocorrelation of the complex gain are important in analysis of modulation on fading channels.

A widely used model for the Doppler power spectrum of a mobile radio channel is the so-called Jakes model [16] where isotropic scattering with a uniform density of scatterers in azimuth around the mobile is considered. In this model the autocorrelation of the time variant transfer function is given as:

$$R_g(\tau) = J_0(2\pi f_d \tau) \tag{3.13}$$

Where $J_0(\ )$ is the zero order Bessel function of the first kind and τ is the time separation. This function specifies the extent to which there is correlation between the channel's response to a sinusoid sent at time t_1 and the response to a similar sinusoid sent at time t_2, where $\tau=t_1-t_2$. to measure $R_g(\tau)$ a single sinusoid may be transmitted and determine the autocorrelation function of the received signal [17].

The Fourier transform of this autocorrelation function yields the Doppler spectrum.

$$\begin{aligned} S_g(\lambda) = & \int_{-f_d}^{f_d} J_0(2\pi f_d \tau) e^{-j2\pi\lambda\tau} d\tau \\ = & \frac{1}{\pi f_d} \frac{1}{\sqrt{1-(\lambda/f_d)^2}} \end{aligned} \tag{3.14}$$

where $\lambda=f_d\cos\theta$ which is the Doppler shift caused by the various scatterers around the mobile.

The power spectrum and the correlation function of *g(t)* is shown in Fig. 3.6 which is derived from isotropic scattering and has a U-shape. For pedestrian use, this spectrum is realistic but for vehicular applications it is not. This is because cars do not usually have large scatterers directly ahead or behind and these are the scatterers that produce the $\pm f_D$ shifts. Another point is that the surroundings are changing and the other cars in the lane facing the mobile also act as scatterers. There is also the fact that in many situations, the environment around the mobile could be dominated by a few large scatterers, rather than a collection of uniformly distributed small scatterers.

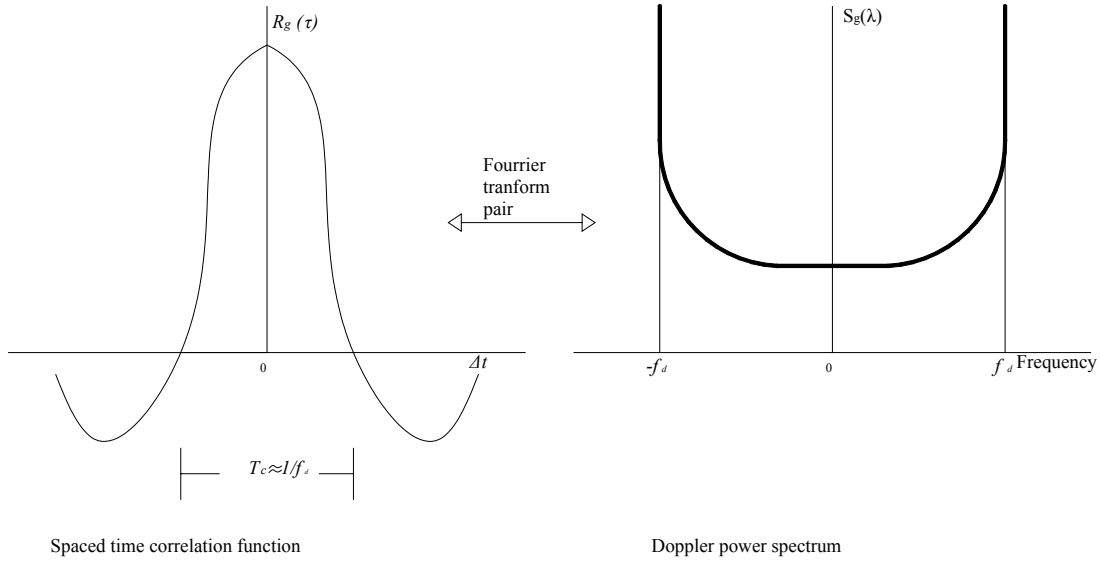

Fig. 3.6 Relationship among channel correlation function and power density functions.

The time over which the complex gain stays roughly constant, so that the signal is relatively undistorted, is termed coherence time. The wider the Doppler spread, the shorter the coherence time, and the signal varies faster. Because the assessments of degree of coherence and distortion are somewhat subjective and because the quantities depend on specific functions, there is no precise definition of coherence time. That is

$$T_c \approx \frac{1}{f_d} \tag{3.15}$$

Clearly a slowly changing channel has a large coherence time and a small Doppler spread.

3.8 Second order statistics of frequency selective, static channels

In frequency selective static channels the signal from the surrounding scatterers arrives at different delays τ_i. In most radio transmission media, the attenuation and phase shift of the channel associated with path delay τ_1 is uncorrelated with the attenuation and phase shift associated with path delay τ_2. This is called uncorrelated scattering (US) and it is assumed that the scattering at different delays is uncorrelated. The distribution of scatterers (density of power) in the delay domain τ is called power delay profile and it is central to any analysis or simulation of delay spread and intersymbol interference.

In order to get a distortion free bandwidth, called the coherence bandwidth, a spaced frequency correlation function should be derived, which is the correlation between the responses due to sinusoids at *f* and *Δf*, when observed at the same time (i.e *Δt*=0)

$$C_g(\Delta f) = \int_{-\infty}^{\infty} P_g(\tau) e^{-j2\pi\Delta f\tau} d\tau \tag{3.16}$$

where the density $P_g(\tau)$ is the power delay profile. Knowledge of $C_g(\Delta f)$ it helps to answer the question what is the correlation between received signals that are spaced in frequency by (Δf). $C_g(\Delta f)$ can be measured by transmitting a pair of sinusoids separated in frequency by (Δf), cross correlating the two separately received signals, and repeating the process many times with ever larger separation (Δf) [17].

The above relationship is depicted graphically in Fig. 3.7. Since $C_g(\Delta f)$ is an autocorrelation function in the frequency variable, it provides a measure of the frequency coherence of the channel. As a result of the Fourier transform relationship between $C_g(\Delta f)$ and $P_g(\tau)$, the reciprocal of the delay spread is a measure of the coherence bandwidth of the channel. Because the assessments of degree of coherence and distortion are somewhat subjective and because the quantities depend on specific functions, there is no precise definition of coherence bandwidth. That is

$$W_c \approx \frac{1}{\tau_d} \tag{3.17}$$

where W_c is the coherence bandwidth. Thus, two sinusoids with frequency separation greater than W_c are affected differently by the channel. When an information bearing signal is transmitted through the channel, if W_c is small in comparison to the bandwidth of the transmitted signal, the channel is frequency selective.

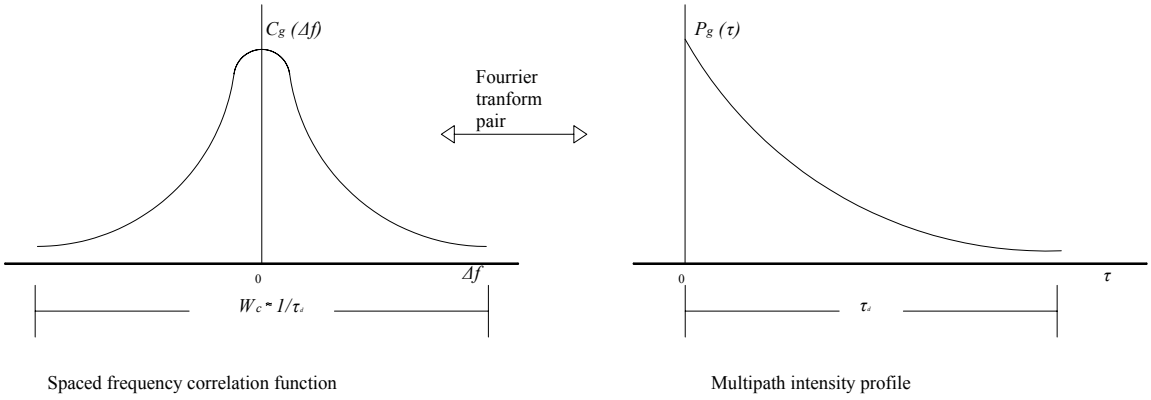

Fig. 3.7 Relationship between frequency correlation and power spectrum.

Some idealized power delay profiles are commonly used in analysis and design. In urban settings it is common for the power delay profile to be approximately

exponential. Another power delay profile commonly used is the two ray model where the arrivals are separated by the maximum delay spread τ_d.

3.9 Second order statistics of time and frequency selective fading channels

In the case where both of the above phenomena are present will be discussed. By assuming that the channels are WSS (scatterers at different Dopplers are uncorrelated) and US (scatterers at different delays are uncorrelated) simplifies the analysis

The average power output of the channel as a function of the time delay τ and the Doppler frequency λ is described by a function called delay - Doppler power density function or **scattering function** of the channel:

$$S_\gamma(\lambda,\tau) = \int_{-\infty}^{\infty}\int_{-\infty}^{\infty} R_G(\Delta t,\Delta f)\cdot e^{-j\cdot 2\pi\cdot\lambda\cdot\Delta t} e^{j\cdot 2\pi\cdot\tau\cdot\Delta f}\, d\Delta t d\Delta f \tag{3.18}$$

3.10 A tapped delay line (TDL) channel model

The tapped delay line is a discrete channel model for frequency selective fading. This model seeks to combat the effect of multipath by using a correlation method to detect the delayed signals individually and then adding them algebraically. In this way, intersymbol interference due to multipath is dealt with by reinserting different delays into the detected signals so that they perform a constructive rather than destructive role. A block diagram of a TDL model is shown in Fig. 3.8. The input signal *s(t)* is sampled at a rate f_s that is high enough to represent the output after Doppler spreading; that is, if the input signal has low pass bandwidth W, then $f_s \geq 2(W+f_d)$. In that way the same sampling rate is used for input and output.

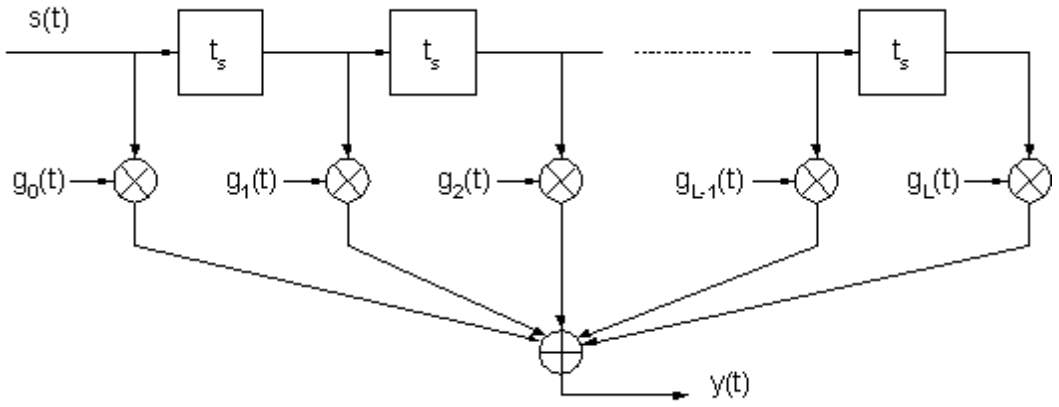

Fig. 3.8 Tapped delay line model

By keeping the WSSUS assumption the coefficients $g_i(t)$ are uncorrelated and because of the central limit theorem are Gaussian. The variances coefficients follow the power delay profile so that:

$$\sigma_{g_i}^2 = K \cdot \int_{it_s}^{(i+1)t_s} P_g(\tau) d\tau \tag{3.19}$$

Where K is a proportionality coefficient and the sampling interval is $t_s=1/f_s$.

The above model may be expressed mathematically with the following equation:

$$y(t) = \sum_{n=0}^{L} s(t - n \cdot t_s) \cdot g_n(t) \tag{3.20}$$

The TDL model has its limitations because the independence of coefficients in the TDL model is expedient, but not completely accurate, even for a WSSUS channel.

In a next chapter an example of such a model will be given and sample plots will be presented.

4 Performance of Star QAM in fading channels

In [18] a simple SER calculation technique adopted in [19] is generalized to derive single-integral closed form expressions of the average SER of Star M-QAM (kAnPSK, M=k×n) in fading channels corrupted by AWGN. Numerical results are computed and plotted for the cases of M=16, 64 and 256. The dependence of error probabilities on fading parameters is also analysed.

4.1 Wireless Channel

The signalling used is Star M-QAM and it is transmitted over a wireless fading channel that is also corrupted by AWGN. The fading is assumed to be slow compared to the signal duration and flat compared to the signal bandwidth. Besides the fading, the signal is also perturbed by AWGN with two-sided PSD $N_0/2$.

It is well known that the symbol error rate performance of M-ary signalling perturbed by stationary AWGN depends only on the instantaneous SNR γ_s describing each symbol [3]. However, in fading channels the instantaneous SNR becomes a random variable and its probability density function for Rician and Nakagami distributions is respectively given by [3]

$$p(\gamma_s) = \left(\frac{1+K}{\overline{\gamma}_s} \right) \cdot \exp\left[-\frac{(1+K)\gamma_s + K\overline{\gamma}_s}{\overline{\gamma}_s} \right] \cdot I_0\left(2\sqrt{\frac{K(1+K)\gamma_s}{\overline{\gamma}_s}} \right) \tag{4.1}$$

$$p(\gamma_s) = \frac{m^m \gamma_s^{m-1} e^{-m\gamma_s / \overline{\gamma}_s}}{\Gamma(m)\left(\overline{\gamma}_s\right)^m} \tag{4.2}$$

where $\overline{\gamma}_s$ is the average instantaneous signal to noise ratio (SNR), K is the Rician parameter, m is the Nakagami parameter, $I_o(x)$ is the modified Bessel function of first kind, and $\Gamma(m)$ is the Gamma function.

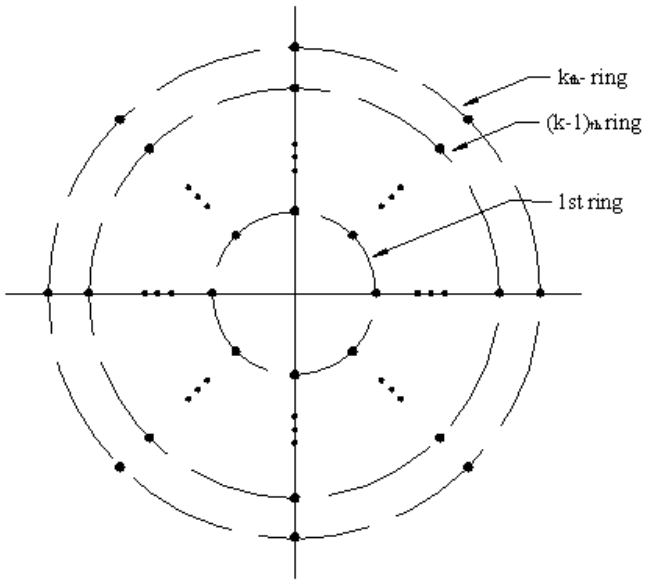

Fig. 4.1 Constellation of M-ary Star QAM

4.2 Error Probability of Star M-QAM

The constellation of star M-QAM (*k*-magnitudes, *n*-phases) is arranged with *n* equidistant signal points per ring on a total of *k* rings with radius *1,2…k* as shown in Fig. 4.1. The original motivation for this type of constellation was to ease carrier recovery, since there are *n* equally valid synchronisation positions as opposed to square M-QAM, which has a number of potential false-lock positions.

Assuming matched filter reception, the symbol signal to noise ratio at the output of the receiver filter is

$$\gamma_s = \frac{S}{N} = \frac{1}{k\sigma^2}\sum_{j=1}^{k} j^2 \tag{4.3}$$

where the average constellation power is $\frac{1^2 + 2^2 + ... + k^2}{k} = \frac{1}{k}\sum_{j=1}^{k} j^2$, and σ^2 is the variance of the thermal noise.

Each constellation point has four neighbours, or three if it belongs to the innermost and outer rings. The distances of each point in the j^{th} inner ring from its neighbours are *{2jsin(π/n), 2jsin(π/n), 1,1}*. The distances of each point in the innermost ring from its neighbours are *{2sin(π/n), 2sin(π/n),1}*. The distances of each point in the outer ring from its neighbours are *{2ksin(π/n), 2ksin(π/n),1}* Thus the average SER is proved to be given by

$$P_s(e/\sigma) = \frac{2(k-1)Q\left(\frac{1}{2\sigma}\right) + \sum_{j=1}^{k} 2Q\left(\frac{2j\sin\frac{\pi}{n}}{2\sigma}\right)}{k} \tag{4.4}$$

The first term of the numerator is the error from the neighbours in the same radius of the circle and the second term is the error from the neighbours from the adjacent phases of the constellation.

Equation (4.4) can be expressed in terms of the inner and outer radius when the ring radius in not fixed to 1. In that case for the 16Star QAM *(k=2, n=8)* and by denoting the inner radius as r_L and the outer radius r_H (4.4) will become

$$P_s(e/\sigma) = \frac{2Q\left(\frac{r_H - r_L}{2\sigma}\right) + 2Q\left(\frac{2r_L\sin\frac{\pi}{8}}{2\sigma}\right) + 2Q\left(\frac{2r_H\sin\frac{\pi}{8}}{2\sigma}\right)}{2} \tag{4.5}$$

By substituting the noise deviation σ in (4.4) with the symbol signal to noise ratio γ_s using (4.3), an alternate expression of SER is derived:

$$P_s(e/\gamma_s) = \frac{2(k-1)Q\left(\frac{1}{2}\sqrt{\frac{k\gamma_s}{\sum_{j=1}^{k} j^2}}\right) + \sum_{j=1}^{k} 2Q\left(\frac{2j\sin\frac{\pi}{n}}{2}\sqrt{\frac{k\gamma_s}{\sum_{j=1}^{k} j^2}}\right)}{k} \tag{4.6}$$

Once the PDF of γ_s is known, the average SER in fading can be calculated by averaging the conditional (on γ_s) SER over the PDF of γ_s

$$P_s(e) = \int_0^{\infty} P_s(e/\gamma_s)\, p(\gamma_s)\, d\gamma_s \tag{4.7}$$

where $P_s(e/\gamma_s)$ is the conditional (on γ_s) SER in non-fading channel corrupted by AWGN.

We now derive the generic expressions for average SER's of coherent star M-QAM over Rician and Nakagami fading channels by using an alternate representation for the Gaussian Q-function [20], which is given by

$$Q(x) = \frac{1}{\pi}\int_0^{\pi/2} e^{\left(-\frac{x^2}{2\sin^2\theta}\right)} d\theta \tag{4.8}$$

By substituting (4.8) into (4.6), the conditional SER for the fading channel of our case is given by

$$P_s(e/\gamma_s)=\frac{2(k-1)}{k\pi}\int_0^{\pi/2}\exp\left(-\frac{k\cdot\gamma_s}{8\sin^2\theta\sum_{j=1}^{k}j^2}\right)d\theta+\sum_{j=1}^{k}\frac{2}{k\pi}\int_0^{\pi/2}\exp\left(-\frac{j^2k\cdot\sin^2\frac{\pi}{n}\gamma_s}{2\sin^2\theta\sum_{j=0}^{k}j^2}\right)d\theta= \tag{4.9}$$

$$=\frac{4B_1}{\pi}\int_0^{\pi/2}\exp\left(-\frac{g_1\cdot\gamma_s}{\sin^2\theta}\right)d\theta+\sum_{j=1}^{k}\frac{4B_2}{\pi}\int_0^{\pi/2}\exp\left(-\frac{g_2\gamma_s j^2}{\sin^2\theta}\right)d\theta$$

where $B_1=\frac{k-1}{2k}$, $B_2=\frac{1}{2k}$ and $g_1=\frac{k}{8\sum_{j=1}^{k}j^2}$, $g_2=\frac{k\sin^2\frac{\pi}{n}}{2\sum_{j=1}^{k}j^2}$

By substituting equations (4.1) and (4.9) into (4.7) we get an expression for the average SER of star M-QAM over Rician fading channel:

$$P_s(e)=\frac{4B_1 l}{\pi}\int_0^{\pi/2}\frac{\sin^2\theta}{h_1(\theta)}\exp\left[-\frac{Kg_1\overline{\gamma}_s}{h_1(\theta)}\right]d\theta+\sum_{j=1}^{k}\frac{4B_2 l}{\pi}\int_0^{\pi/2}\frac{\sin^2\theta}{h_{2,j}(\theta)}\exp\left[-\frac{Kg_2\overline{\gamma}_s j^2}{h_{2,j}(\theta)}\right] \tag{4.10}$$

where l=K+1 and $h_1(\theta)=l\sin^2\theta+g_1\overline{\gamma}_s$, $h_{2,j}(\theta)=l\sin^2\theta+j^2g_2\overline{\gamma}_s$

The substitution of (4.2) and (4.9) into (4.7) yields the following expression for average SER of star M-QAM over Nakagami-m fading channel:

$$P_s(e)=\frac{m^m 4B_1}{\pi}\int_0^{\pi/2}\left[\frac{\sin^2\theta}{m\sin^2\theta+g_1\overline{\gamma}_s}\right]^m d\theta+\sum_{j=1}^{k}\frac{m^m 4B_2}{\pi}\int_0^{\pi/2}\left[\frac{\sin^2\theta}{m\sin^2\theta+j^2g_2\overline{\gamma}_s}\right]^m d\theta \tag{4.11}$$

The above expressions (4.10) and (4.11) are high SNR approximations because only the distances to the immediate neighbours were considered in equation (4.4) were the average SER was initially calculated. An error that occurs to an immediate neighbour dominates in the high SNR regime, but at low SNRs there is a probability that an error occurs to another more distant point of the constellation. This error is not negligible but it is not taken into account in the derivation of the above equations. In the following chapter a simulation of a fading channel under Rician fading will be carried out and the validity of the above results will be confirmed.

4.3 Numerical Results

The final SER expressions for Star M-QAM are computed numerically for different values of M (M=16, 64, 256) while keeping the number of phases constant (n=8) and results are plotted in Fig. 4.2 and Fig. 4.3 for Rician and Nakagami fading channels respectively. The results are plotted for various values of *K* and *m* in order to show the dependency of SER on Rician parameter *K* and Nakagami parameter *m*. It can be seen that for a fixed value of M, as *K* or *m* increases, less power is needed in order to

achieve the same SER. This happens because as K or m increases the fading depth decreases. It is also shown that for fixed K or m as M increases, SNR has to be increased to keep the SER constant, which is exactly what one can expect from the theory of M-ary modulation techniques.

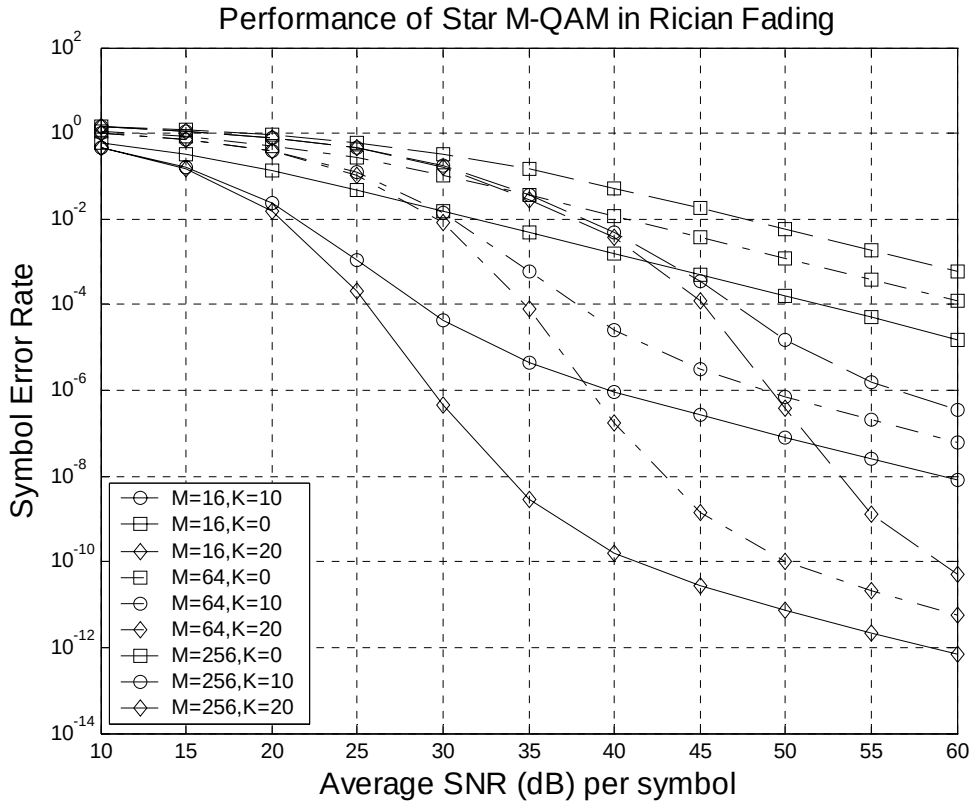

Fig. 4.2 Average SER of coherent Star M-QAM in Rician fading channels

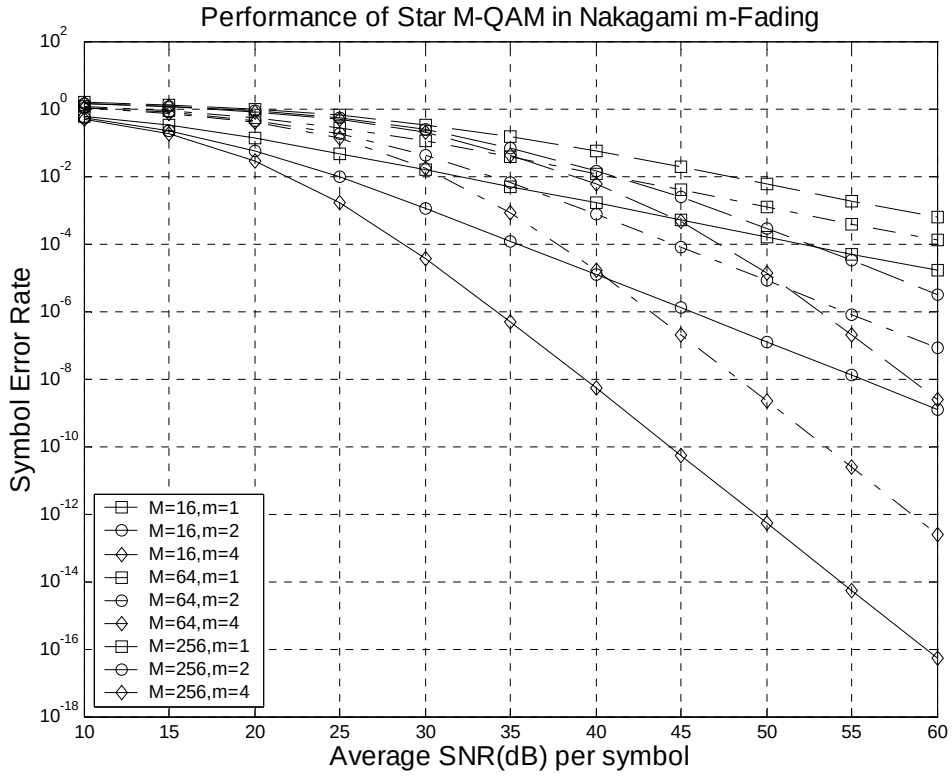

Fig. 4.3 *Average SER of coherent Star M-QAM in Nakagami-m fading channels*

Error rate performance of coherent Star M-QAM in slow, flat, fading channels is presented in terms of a single finite integral with an integrand composed of elementary (exponential and trigonometric) functions. The solutions are simple enough to allow numerical computation for cases of practical interest and general enough so that they include AWGN [$K = \infty$ in (4.1), $m = \infty$ in (4.2)] and Rayleigh fading plus AWGN [$K = 0$ in (4.1) $m=1$ in (4.2)].

5 Simulating fading channels

Simulation is a tool for system design and evaluation. Of course, simulation is often used in industry to evaluate systems for which analytical results are not available due to numerous implementation effects. In this chapter simulations are used to get results on the bit error rate of Star M-QAM in flat fading channels.

5.1 Generation of complex gain

As it was seen in a previous chapter, fading channels are characterized by the multiplication of a complex number to the signal. In order to simulate a fading channel a reliable way is needed to generate those complex gains with the right properties. The real and imaginary components must be both Gaussian with the same autocorrelation function, and independent to each other. Additionally different complex gain generators in a frequency selective channel model should be independent.

The signal strength in dB along an arbitrary direction for an unmodulated carrier may be visualized by using the Jake's complex gain generator for isotropic scattering [16]

Jakes method is a way to simulate fading channels by generating channel complex gain samples which are statistically reliable, and computationally undemanding. In order to produce a Gaussian process with statistics corresponding to isotropic scattering, it mimics the model Jakes used to calculate the power spectrum in the first place – rays arriving uniformly from all directions with the same power. Computationally the method is very attractive because the processing load per sample is reasonable, its structure lends itself to real time DSP implementation, it can be run forward or backward in time, and the time step size can be varied at will. The original algorithm had a problem with persistent correlation between supposedly independent generators. The modification in [21] got around part of the difficulty, but introduced other forms of correlation, as well as non-WSS behavior, which together make it unsuitable for simulation.

This problem is solved by using a Jakes - like generator [15] which is a good approximation to a Gaussian random process, it is band-limited and wide sense stationary, and it is easy to create multiple uncorrelated generators. The only drawback is that more rays are required in order to achieve the desired power spectrum.

If it is assumed that there are N_s scatterers equispaced in azimuth around the mobile, with all scattered signals have the same amplitude, but random phases φ_i, the generated complex gain will be the sum of the scattered signals.

$$g(t) = \frac{1}{\sqrt{N_s}} \cdot \sum_{0}^{N_s-1} e^{j\varphi_i} \cdot e^{j2\pi \cdot f_d \cdot t\cos(\theta_i)} \tag{5.1}$$

From the previous chapters it was assumed that the process *g(t)* is wide sense stationary. In order to make sure that *g(t)* is WSS a test during simulation should be carried out. This process will be WSS if the real and imaginary components of *g(t)* are uncorrelated and have the same autocorrelation functions. This is:

$$\begin{aligned} E(g(t)\cdot g(t-\tau)) &= 0 \\ \frac{1}{N_s}\sum_{i=0}^{N_s-1}\sum_{n=0}^{N_s-1} e^{j(\varphi_i+\varphi_n)} \cdot E(e^{j(\omega_i+\omega_n)t}) \cdot e^{-j\omega_n\tau} &= 0 \end{aligned} \tag{5.2}$$

Where $\omega_i = 2\pi f_d \cos(\theta_i)$. The above average will be zero provided that $\omega_n \neq 0$ and $\omega_i \neq \omega_n$. Since the Doppler shifts are determined by the arrival angles, $\theta_i = \theta_0 + \frac{2\pi}{N_s} \cdot i$, the zero average is achieved by ensuring that the number of rays N_s is odd and no arrival angle, θ_0, is equal to $\pm\pi/2$. A Matlab function is written in order to ensure the above conditions are kept.

The autocorrelation function of the Jakes model as it was mentioned in a previous chapter (3.13) is a Bessel function J_0 and the simulation should give complex gains with autocorrelation that resembles this function, and have variance 0.5 so that it doesn't change the signal power passing through the channel. That is:

$$\begin{aligned} R_g(\tau) &= E(g(t)\cdot g(t-\tau)^*) \\ &= \frac{1}{N_s}\cdot\sum_{i=0}^{N_s-1}\sum_{n=0}^{N_s-1} e^{j\cdot(\varphi_i-\varphi_n)} E(e^{j\omega_i t} e^{-j\omega_n(t-\tau)}) \\ &= \frac{1}{N_s}\cdot\sum_{i=0}^{N_s-1}\sum_{n=0}^{N_s-1} e^{j\cdot(\varphi_i-\varphi_n)} \cdot \delta(i,n) \cdot e^{j\omega_n\tau} \\ &= \frac{1}{N_s}\cdot\sum_{n=0}^{N_s-1} e^{j\omega_n\tau} \\ &= \frac{1}{N_s}\cdot\sum_{n=0}^{N_s-1} e^{j2\pi\cdot f_d\tau\cos(\theta_n)} \\ &\approx J_0(2\pi\cdot f_d\tau) \end{aligned} \tag{5.3}$$

Since the summation in the second last line is a discrete approximation to an integral that is one definition of the J_0 function:

$$J_0(2\pi f_d \tau) = \frac{1}{2\pi}\int_{-\pi}^{\pi} e^{j2\pi \cdot f_d \tau \cos(\theta)} d\theta \qquad (5.4)$$

The approximation is quite good for just a few arrivals and its quality depends on the offset angle θ_0. The best case is where $\theta_0=0$ and the worst case $\theta_0=\pi/2N_s$. The approximation is quite good out to about $f_d\tau$=2 to 4 for N_s=15 rays, and this interval of good fit may be doubled by doubling the number of rays. In the original algorithm of Jakes the interval of good representation is twice as large than the used method but the WSS behavior is better in the method used in this simulation.

The complex gain may now be derived by applying to (5.1) the randomized phases φ_n, and Doppler shifts ω_i which are generated by taking in mind the WSS behavior.

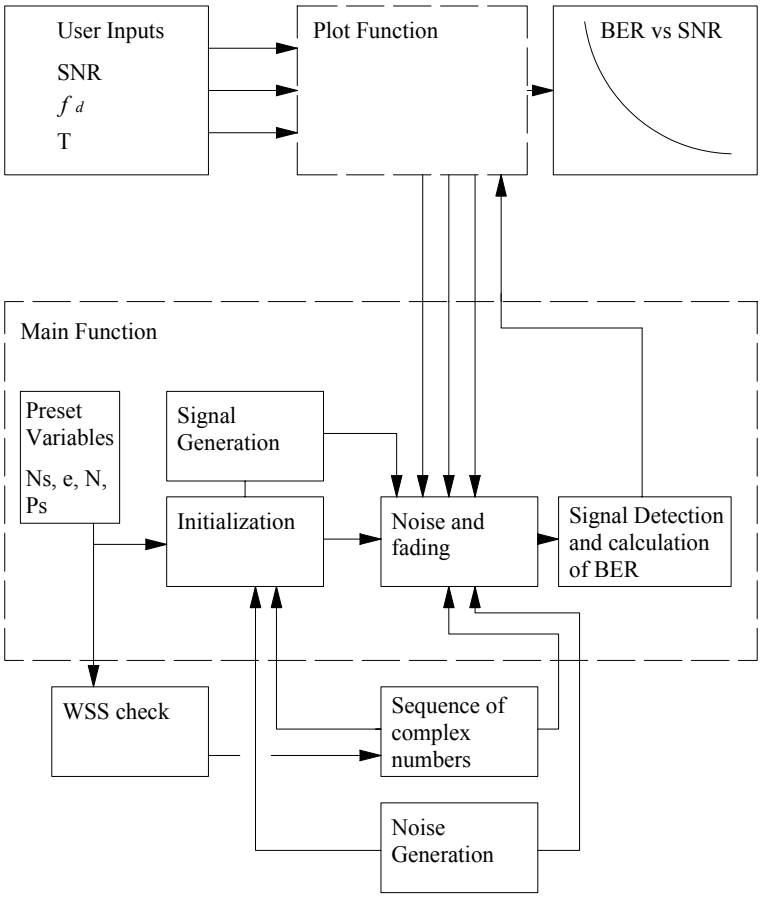

Fig. 5.1 Flow Diagram of simulation of slow and fast fading channel

5.2 Simulation of Differentially encoded 16 Star QAM in slow and fast fading channels

The complex gains generated in the previous section will be used for the simulation of the differentially encoded 16 Star QAM over a fading channel. For flat fading the

received signal at the output of the fading channel and before addition of receiver noise is $y(t)=g(t)\cdot s(t)$. So the power of the received signal will be:

$$P_y = \frac{1}{2}E\left[\left(|y(t)|\right)^2\right] = \frac{1}{2}E\left[\left(|g(t)|\right)^2\right]\cdot E\left[\left(|s(t)|\right)^2\right] = 2\sigma_g^2 \cdot P_s \qquad (5.5)$$

Since the complex gains $g(t)$ have variance $\sigma_g^2 = ½$ the received power will remain unchanged by the complex gain power.

The fundamental SNR per bit parameter is SNR=E_b/N_0. For the case of 16 Star QAM where $E_s=4E_b$ and $E_s=P_sT$ we have that $N_0= P_sT/4SNR$. By assuming that the bandwidth is twice the symbol rate $W=2/T$ and the sampling rate is twice the bandwidth $2W=4/T$ we operate at $N_{ss}=4$ samples per symbol.

The receiver noise will have variance $\sigma_n^2 = 2N_0W$ and by substituting the above we get:

$$\sigma_n^2 = \frac{N_{ss}}{T}\frac{P_sT}{4\cdot SNR} = N_{ss}\frac{P_s}{4\cdot SNR} \qquad (5.6)$$

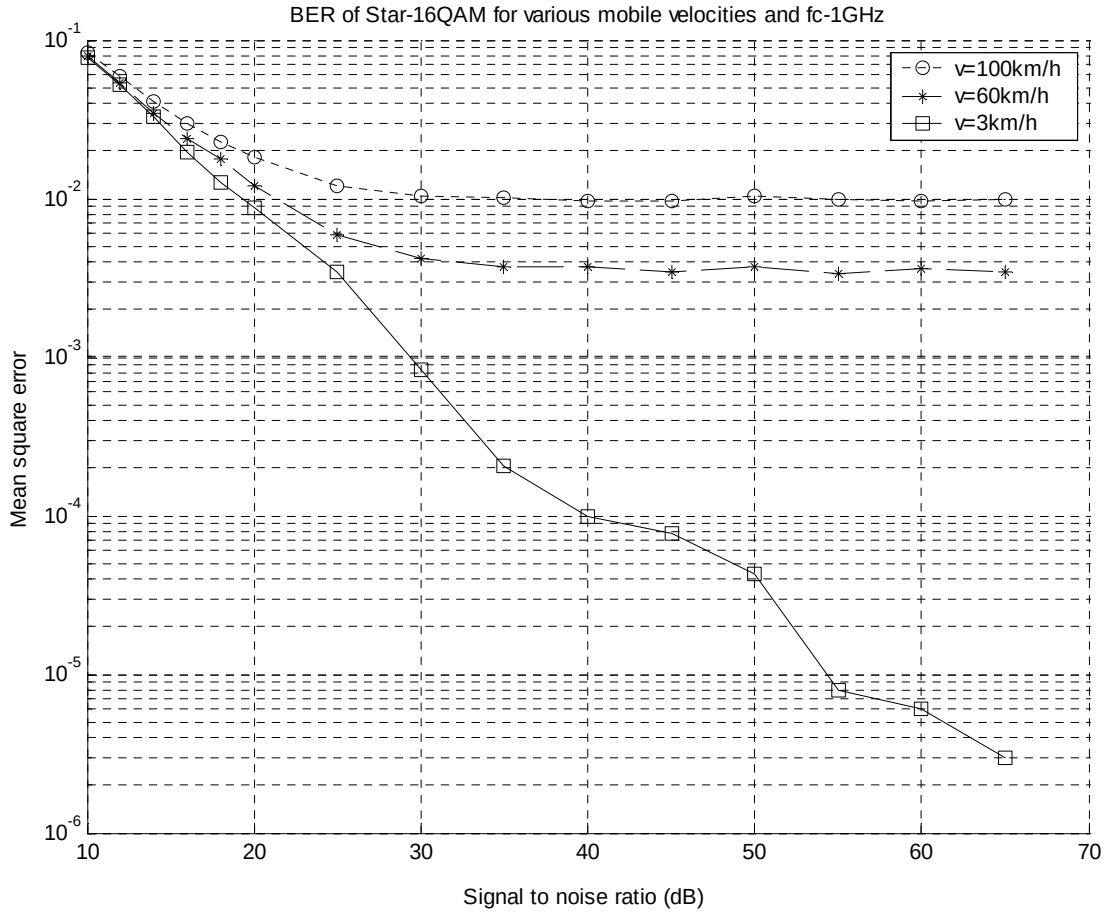

Fig. 5.2 BER of Star 16QAM for various mobile velocities and f_c=1GHz

The parameter that distinguishes slow from fast fading as it was mentioned in a previous chapter is f_dT which is an input to the simulation. If f_dT <<1 the fading is slow, otherwise it is fast. Below in Fig. 5.1 there is a flow diagram of the simulation. Simulations were carried out for various values of f_dT (T=10^{-4}sec), ($f_d=f_cv/c$) and N=1.000.000 symbols, and the signal was detected by using a matched filter. Matlab code is included in Appendix and graphic results are shown below for Bit Error Rate versus SNR.

As it can be seen in Fig. 5.2 as the velocity of the mobile increases the performance of the channel decreases. For carrier frequency 1GHz and pedestrian speed of v=3km/h the fading is slow and the performance of the channel increases as the SNR increases but for greater speeds where the fading is fast there is an error floor which is not corrected as the SNR increases.

In Fig. 5.3 where the carrier frequency is increased and hence the Doppler frequency is increased the same behavior exists only that the performance of the channel is worst.

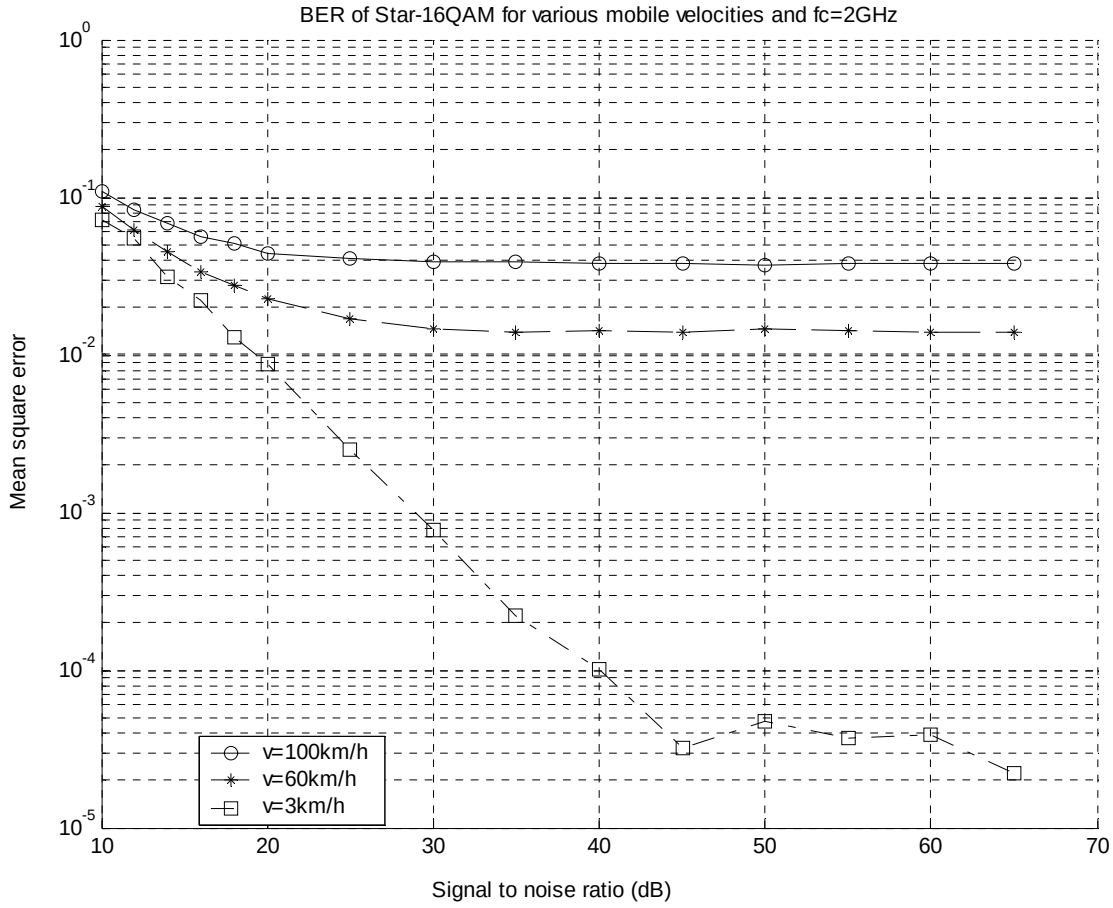

Fig. 5.3 BER of Star 16QAM for various mobile velocities and f_c=2GHz

5.3 Comparison of simulations with theoretical results

In order to check the validity of the results obtained in chapter 4 simulations were carried out using a Rician fading channel for various values of K (K=0, K=10, K=20). The method used was the same as in the previous sections with only difference that the Jakes method for generating the complex gain was substituted by a function which generated Rician distributed complex numbers. The number of symbols that the simulation was run was N=1.000.000 so the error accuracy that could be achieved was up to 10^{-6}. Because the error accuracy of the theoretical results for high SNR was up to 10^{-12} for K=20 the results were plotted for SNRs that the SER were not smaller than 10^{-6}.

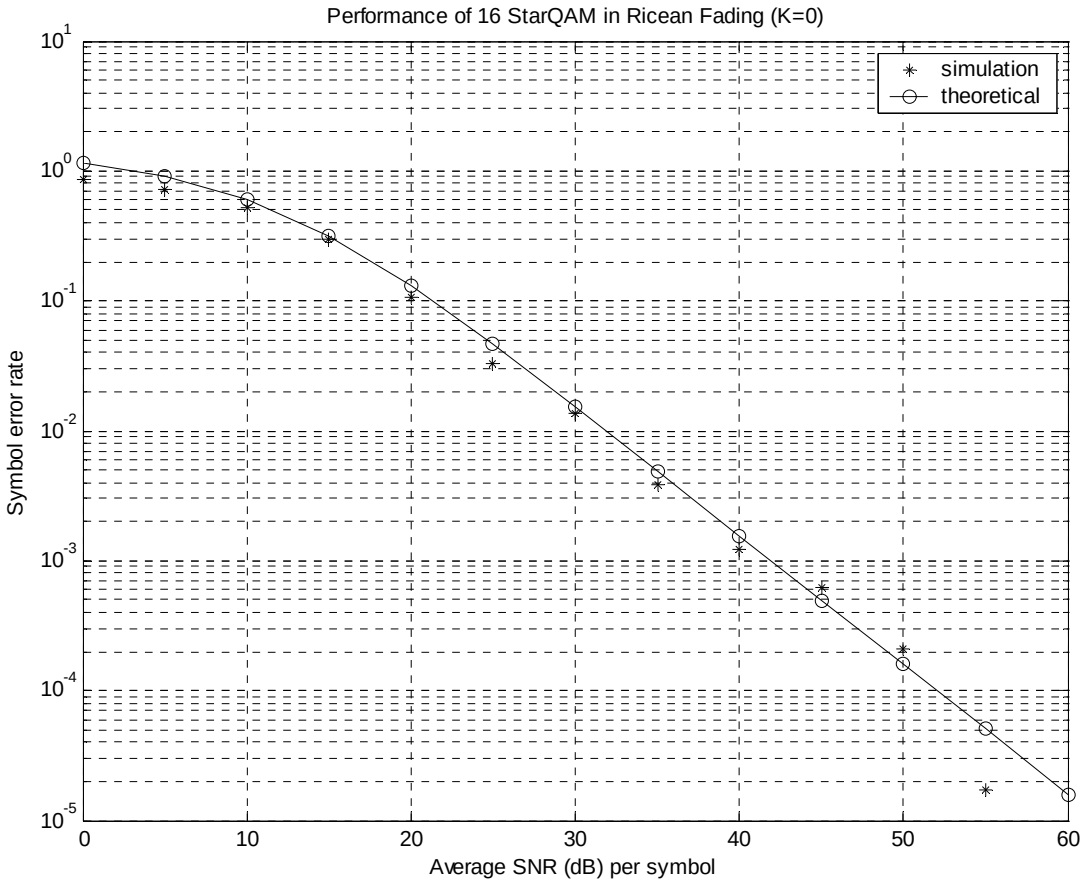

Fig. 5.4 Comparison of simulation with theoretical results for 16 Star QAM in a Rician fading channel for K=0, (Rayleigh)

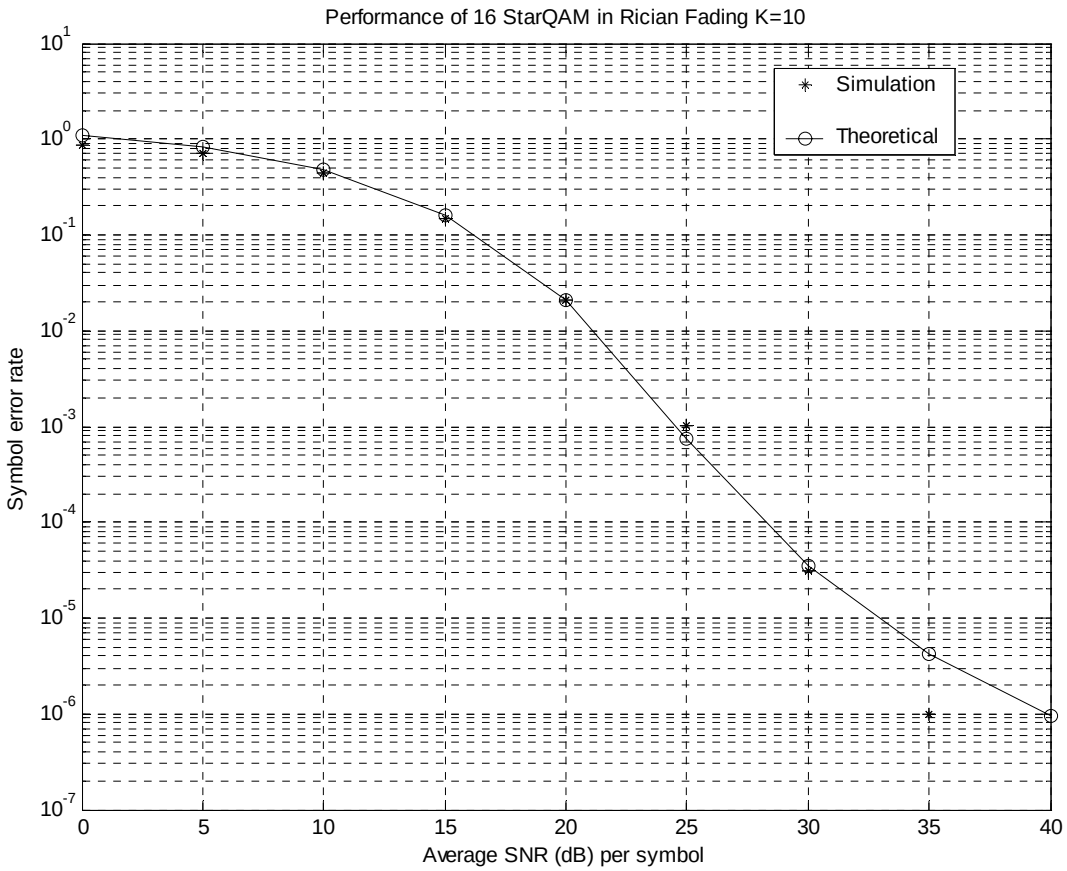

Fig. 5.5 Comparison of simulation with theoretical results for 16 Star QAM in a Rician fading channel for K=10

It can be seen in Fig. 5.4, Fig. 5.5, Fig. 5.6 that the simulation results follow the theoretical equation for a Rician slowly, flat fading channel. In chapter 4 it was mentioned that the approximation of the SER of Star QAM was a high SNR approximation which is confirmed by the simulations. It can be seen in Fig. 5.4 were the fading is more severe, that at low SNRs (0-10dB) the results are not the same for the simulation and the theoretical curve. For higher K, Fig. 5.5, Fig. 5.6, this difference is smaller since the fading is less. These results are presented with more clarity in Fig. 5.7, Fig. 5.8, and Fig. 5.9 were the symbol error rate is shown only for low SNRs

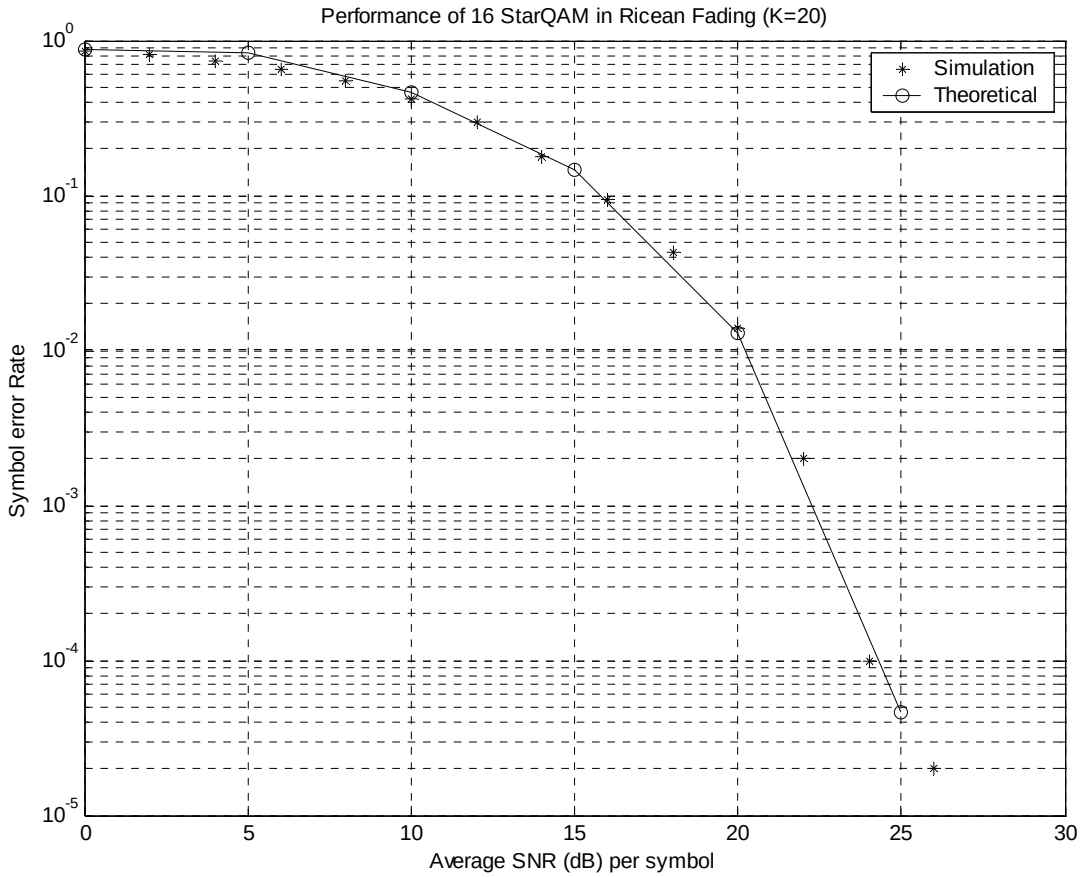

Fig. 5.6 Comparison of simulation with theoretical results for 16 Star QAM in a Rician fading channel for K=20, (nearly Gaussian)

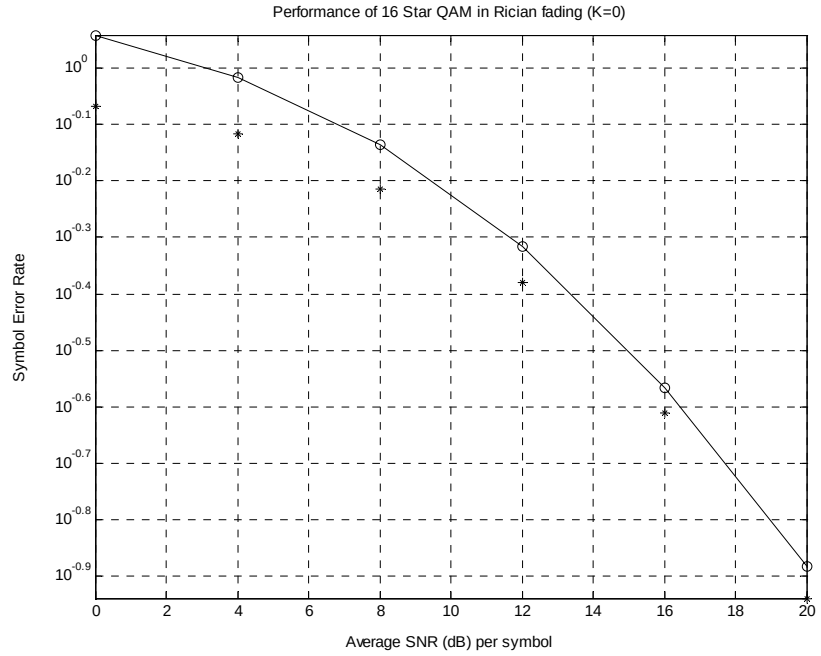

Fig. 5.7 Comparison of simulation with theoretical results for 16 Star QAM in a Rician fading channel for K=0, for low SNRs (0-20dB)

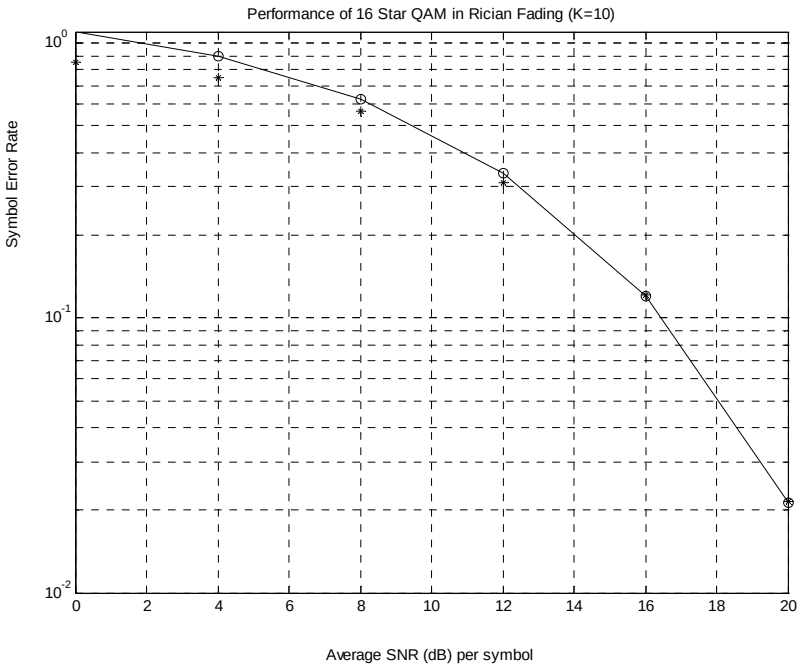

Fig. 5.8 *Comparison of simulation with theoretical results for 16 Star QAM in a Rician fading channel for K=10, for low SNRs (0-20dB)*

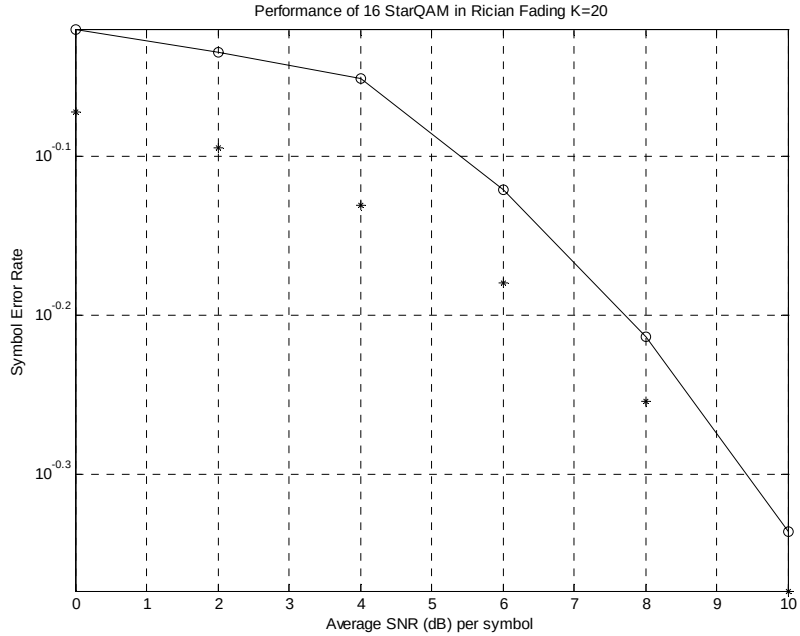

Fig. 5.9 *Comparison of simulation with theoretical results for 16 Star QAM in a Rician fading channel for K=20, for low SNRs (0-10dB)*

5.4 Example of a frequency selective channel using a TDL model.

In this section a transmitted signal will be created and it will be passed through a TDL channel. Graphs of the input and output signal will be presented and it will be shown what effect has the delay spread and the Doppler frequency at the output signal.

By using a phase modulated carrier with a cosine:

$$s(t) = e^{j2\pi \cdot f_d \cos(2\pi \cdot f_m t)} \tag{5.7}$$

and choosing the modulation frequency f_m =10 KHz, the sampling rate $1/t_s=32f_m$ and the modulation index $f_d=0.4$.

by assuming a linear decay in the power delay profile:

$$P_g(\tau) = \frac{2}{\tau_d} \cdot \left(1 - \frac{\tau}{\tau_d}\right) \quad 0 \leq \tau < \tau_d \tag{5.8}$$

So that the area $\sigma_g^2=1$.

The number of taps in the model will be the division of the delay spread over the sampling time rounded up, and it expresses the number of samples that there will still be information of the transmitted symbol after it was first received.

$$N_t = \frac{\tau_d}{t_s} \tag{5.9}$$

The standard deviation per tap is

$$\sigma_{g_n} = \sqrt{\int_{nt_s}^{(n+1)t_s} P_g(\tau) d\tau} \tag{5.10}$$

where $n=0,\ldots,N_t-1$

The complex gain is generated in the same way as in the flat fading case and it is remains constant for each tap.

The channel output is given by the equation

$$y(t) = \sum_{n=0}^{\min(N_t-1,t)} s(t - n \cdot t_s) \cdot g_n(t) \tag{5.11}$$

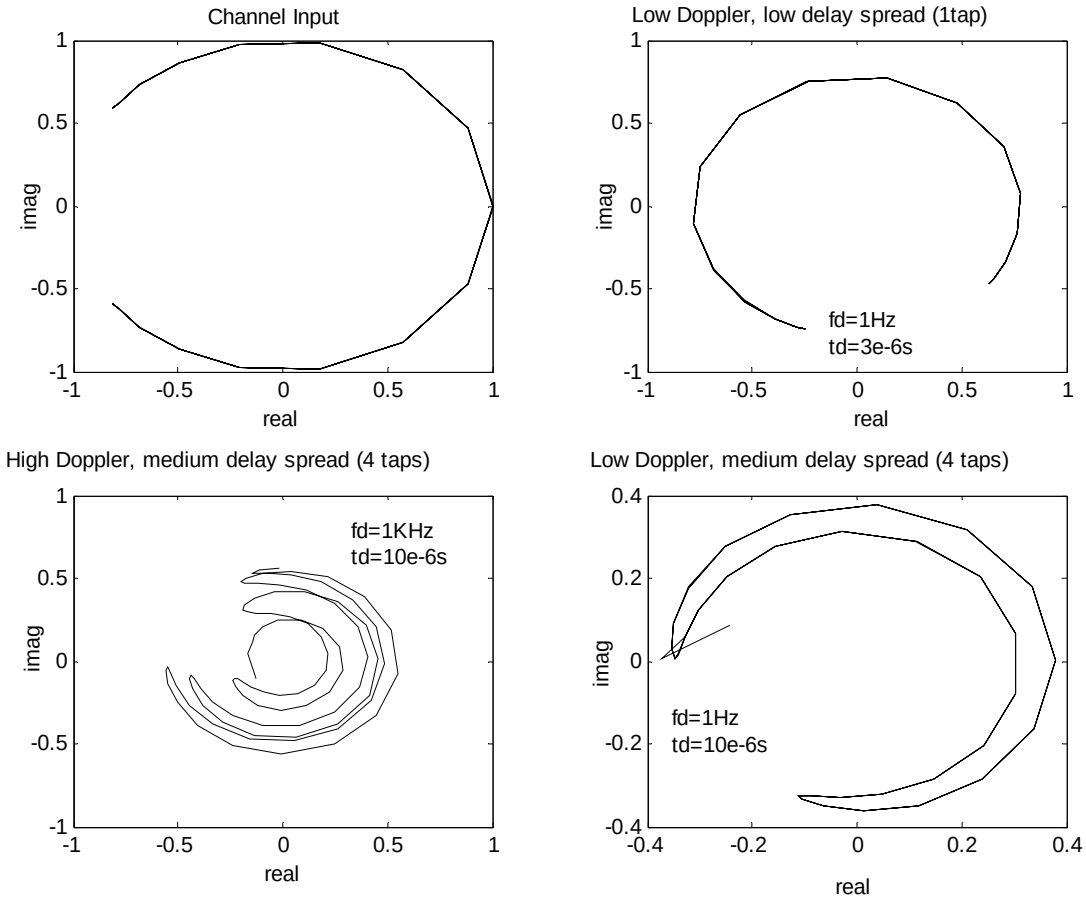

Fig. 5.10 Comparison of input and output of a TDL channel

From Fig. 5.10 it can be seen that a delay spread of τ_d=10μs causes considerable damage, even to a 10KHz signal, but a Doppler of 1 Hz does not make the output aperiodic over this short observation interval. In the lower left graph where the Doppler frequency is 1 KHz it can be seen that the damage to the signal is worst even if the number of taps are the same. In the top right graph where Doppler frequency and delay spread are low the signal is not that much disturbed.

6 Conclusions

In this work performance Star QAM over fading channels was studied. Initially PAM and PSK signals where explained and performance curves over AWGN channels where given. The QAM modulation was then described and it was made obvious that QAM is generated by combining PAM and PSK signals together. Fading channels where then described and all possible form of fading where presented. It was made clear that fast and slow fading is a consequence of vehicular motion and frequency flat and frequency selective fading is a consequence of the surroundings. First and second order statistics of fading were given which where later used in simulations.

Afterwards closed form expressions of the average SER for Star MQAM slow-flat fading channels were derived and performance curves were given for various Ricean and Nakagami-m statistics. Finally simulations were run for Star 16QAM in flat fading channels and performance curves were given for slow and fast fading. Also an example of frequency selective signal was presented and the distortion to the output signal was shown.

Further study of the above work may include simulations for frequency selective Star QAM channels and application of methods to mitigate the consequences of fading.

Rererences

[1] Simon K. Marvin, Alouini Mohamed-Slim., 'Digital Communication over fading channels', 2nd ed. 2005 Wiley Interscience

[2] Haykin Simon., 'Communication Systems' 4th ed. 2001 Wiley

[3] Proakis, J. G.: 'Digital Communications' McGraw-Hill, New York, 1995 3rd ed.

[4] Fortune, P. M., Hanzo, L., and Steele, R.: 'Transmission of SBC speech nia 16-level QAM over mobile radio channels' Proc Globecom 88, pp.832-836

[5] Issman, E., and Webb, W.T.: 'Carrier recovery for 16-level QAM in mobile radio'. IEE Colloquium in Multi-level modulation techniques for point- to – point and mobile radio, March 1990, paper 9

[6] Webb, W.T., Hanzo, L., Steele, R.,: 'Bandwidth efficient QAM schemes for Rayleigh fading channels'. IEE Proceedings Vol.138, No.3, June 1991, pp169-175

[7] Adachi F. Sawahashi M., : ' Decision feedback differential detection of differentially encoded 16APSK signals.' IEEE Trans. on Commun., Vol44: 416-418, Aug. 1996.

[8] Adachi F. Sawahashi M., : 'Performance analysis of various 16 level modulation schemes under Rayleigh fading' Electron. Lett. Vol 28, pp. 1579-1581, Nov. 1992

[9] Wei R, Lin M.:'Modified decision feedback differential detection for differentially encoded 16 APSK signals.' Electronics Letters, 34(4):336-337,. 1998

[10] Schober R., Gerstacker W. Huber J., : 'Decision-feedback differential detection scheme for 16 DAPSK.' Electronics Letters, 34(19):1812-1813, Sep1998

[11] Adachi F.: 'Error rate analysis of Differentially encoded and detected 16APASK under Rician fading' IEEE Trans. on Veh. Tech, 45:1-11, Feb 1996.

[12] Dong X. Tjhung T. Adachi F. : 'Error Probability analysis for 16 Star-QAM in frequency-Selective Rician Fading with diversity reception', IEEE Trans. on Veh. Tech., Vol.47 No3, pp.924-935, Aug.1998

[13] Hanzo L. Webb W. Keller T., 'Single- and Multi –Carrier Quadrature Amplitude Modulation', Wiley 2000

[14] Proakis, J. G. Salehi M., ‘Communication Systems Engineering’ Prentice Hall, International Ed.

[15] Cavers K. James, ‘Mobile Channel Characteristics’ Kluwer Academic Publishers 2000.

[16] Jakes, W. C. ‘Microwave Mobile Communications’ Wiley, New York, 1974.

[17] Sklar, B. ‘Rayleigh fading channels in mobile digital communication systems Part I: characterization’ IEEE Communications Magazine, July 1997.

[18] Barbounakis I. Papadakis A, ‘Closed form SER Expressions for Star MQAM in frequency non-selective Rician and Nakagami-m channels’ Int. J. Electron. Commun. (AEU), article in press.

[19] Burr, A. ‘Performance of 16-QAM and Star QAM on a non-linear channel’ COST 259 TD(99) 102 Leidschendam, Nederlands, 23-24th September 1999

[20] Simon M. K. and Divsalar D., ‘Some new twists to problems involving the Gaussian probability integral’ IEEE Trans. Commun., vol.46, Feb. 1998 pp. 200–210

[21] Dent, P. Bottomley, G. E. Croft, T., ‘Jakes fading model revisited’, IEE Electronics Letters, Vol.29, no.3, pp.1162-1163, June1993